

# Cortical layer-specific modulation of neuronal activity after sensory deprivation due to spinal cord injury

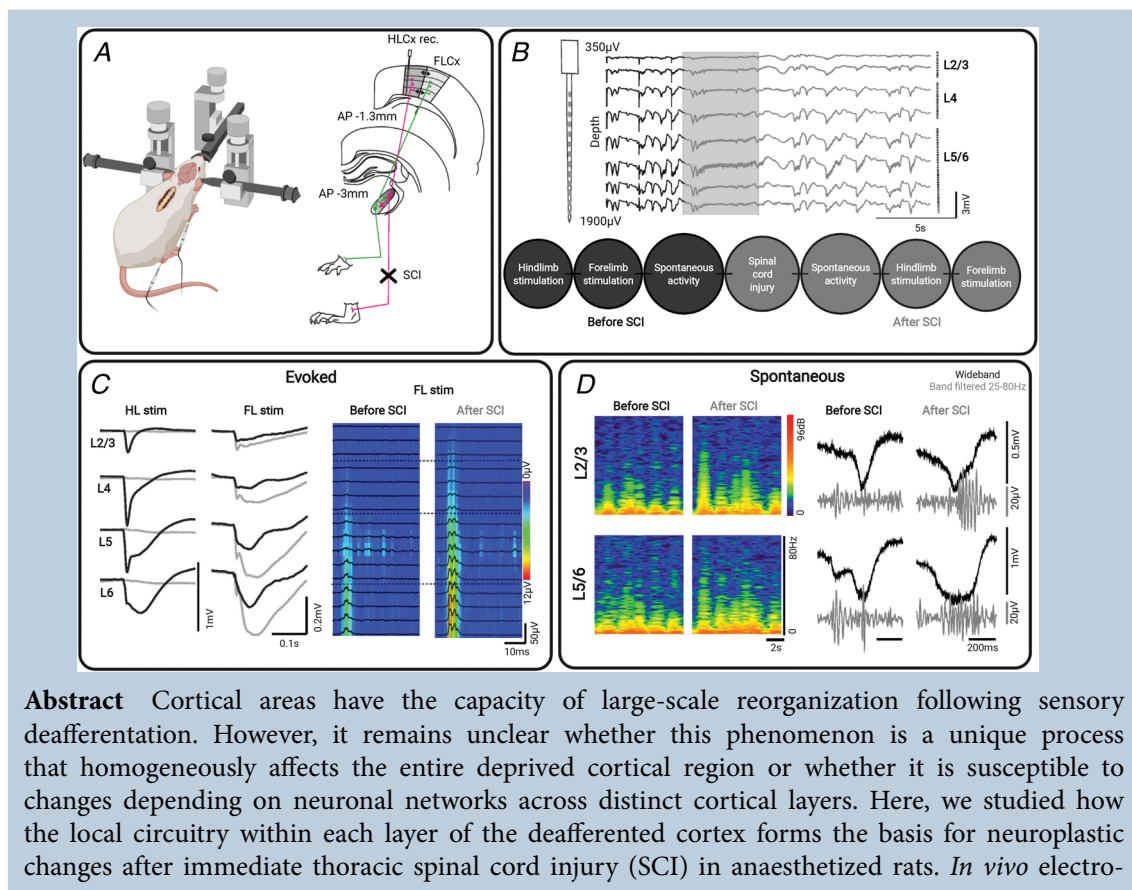
Marta Zaforas<sup>1,2</sup> , Juliana M. Rosa<sup>1</sup> , Elena Alonso-Calviño<sup>1</sup> , Elena Fernández-López<sup>1</sup> ,  
Claudia Miguel-Quesada<sup>1</sup> , Antonio Oliviero<sup>2</sup>  and Juan Aguilar<sup>1</sup> 

<sup>1</sup>Experimental Neurophysiology and Neuronal Circuits Group, Research Unit, Hospital Nacional de Paraplégicos – SESCAM, Toledo, 45071, Spain

<sup>2</sup>FENNSI Group, Hospital Nacional de Paraplégicos – SESCAM, Research Unit, Toledo, 45071, Spain,

Edited by: Harold Schultz & Richard Carson

The peer review history is available in the Supporting Information section of this article (<https://doi.org/10.1113/JP281901#support-information-section>).



**Abstract** Cortical areas have the capacity of large-scale reorganization following sensory deafferentation. However, it remains unclear whether this phenomenon is a unique process that homogeneously affects the entire deprived cortical region or whether it is susceptible to changes depending on neuronal networks across distinct cortical layers. Here, we studied how the local circuitry within each layer of the deafferented cortex forms the basis for neuroplastic changes after immediate thoracic spinal cord injury (SCI) in anaesthetized rats. *In vivo* electro-

M. Zaforas and J. M. Rosa contributed equally to this study.

This article was first published as a preprint: Zaforas M, Rosa JM, Alonso-Calviño E, Fernández-López E, Miguel-Quesada C, Oliviero A, Aguilar J. 2021. Cortical layer-specific modulation of neuronal activity after sensory deprivation due to spinal cord injury. bioRxiv. <https://doi.org/10.1101/2020.12.28.424612>

physiological recordings from deafferented hindlimb somatosensory cortex showed that SCI induces layer-specific changes mediating evoked and spontaneous activity. In supragranular layer 2/3, SCI increased gamma oscillations and the ability of these neurons to initiate up-states during spontaneous activity, suggesting an altered corticocortical network and/or intrinsic properties that may serve to maintain the excitability of the cortical column after deafferentation. On the other hand, SCI enhanced the infragranular layers' ability to integrate evoked sensory inputs leading to increased and faster neuronal responses. Delayed evoked response onsets were also observed in layer 5/6, suggesting alterations in thalamocortical connectivity. Altogether, our data indicate that SCI immediately modifies the local circuitry within the deafferented cortex allowing supragranular layers to better integrate spontaneous corticocortical information, thus modifying column excitability, and infragranular layers to better integrate evoked sensory inputs to preserve subcortical outputs. These layer-specific neuronal changes may guide the long-term alterations in neuronal excitability and plasticity associated with the rearrangements of somatosensory networks and the appearance of central sensory pathologies usually associated with spinal cord injury.

(Received 11 May 2021; accepted after revision 19 August 2021; first published online 21 August 2021)

**Corresponding author** J. Aguilar: Experimental Neurophysiology and Neuronal Circuits Group, Research Unit, Hospital Nacional de Paraplégicos – SESCAM, Toledo, 45071 Spain. Email: jdaguilar@sescam.jccm.es

**Abstract figure legend** (A) Experimental design: on left panel, anesthetized animal placed in stereotaxic frame with spinal cord exposed; on right panel draw, schematic representation of experimental approach: multielectrode probe placed in hindlimb somatosensory cortex to obtain electrophysiological recordings from six cortical layers in response to forelimb stimulation under control conditions and immediately after spinal cord injury. (B) Top, example of spontaneous cortical activity recorded before, during (darker square) and immediately after a spinal cord injury (SCI) showing simultaneous recordings from the six cortical layers were using the 32 channels probe; Bottom, schematic timeline of recording sessions to obtain cortical evoked responses to peripheral stimulation of forelimb and Hindlimb under control conditions (dark circles) and after spinal cord injury (grey circles). (C) Left panel, somatosensory evoked potentials across cortical layers in response to hindlimb (HL) stimulation and forelimb (FL) stimulation under control conditions (black traces) and after SCI (grey traces) showing increased response magnitudes to FL stimulation after SCI. Somatosensory responses in HL cortex to FL stimulation before and after SCI showing increased response magnitudes across layers after SCI (black traces are averaged rectified multiunit activity, and color map). (D) Power spectrum of frequencies (0–80Hz) obtained from cortical spontaneous activity in cortical layers 2/3 (top) and L5/6 (bottom) before and after SCI, increased gamma frequency was observed in supragranular layers. Right panel, representative examples of cortical up-states raw signal (black) and filtered signal in range of gamma frequency (grey) from cortical layers 2/3 (top) and L5/6 (bottom). Gamma activity was increased in cortical layers 2/3 after SCI. Our results show that a spinal cord injury induce immediate physiological changes, which are different depending on cortical layers in deafferented somatosensory cortex.

### Key points

- Sensory stimulation of forelimb produces cortical evoked responses in the somatosensory hind-limb cortex in a layer-dependent manner.
- Spinal cord injury favours the input statistics of corticocortical connections between intact and deafferented cortices.
- After spinal cord injury supragranular layers exhibit better integration of spontaneous corticocortical information while infragranular layers exhibit better integration of evoked sensory stimulation.
- Cortical reorganization is a layer-specific phenomenon.

## Introduction

Spinal cord injury (SCI) produces a physical disconnection between the brain and spinal cord regions below the injury level. Such deafferentation interrupts the sensory information ascending towards the somatosensory cortex, which promotes extensive cortical reorganization (CoRe) of sensorimotor areas (Jain *et al.* 1998, 2008; Curt *et al.* 2002; Endo *et al.* 2007; Ghosh *et al.* 2010). Similar cortical rearrangements following sensory deprivation have also been described in the visual (Griffen *et al.* 2017) and auditory (Bola *et al.* 2017) cortex, indicating that CoRe remapping is a physiological phenomenon across brain regions. In the case of a SCI, the importance of CoRe lies in the crucial role that it plays in functional recovery (Kao *et al.* 2009; Manohar *et al.* 2017). On the other hand, an excessive or maladaptive remapping is implicated in the generation of associated pathologies such as neuropathic pain and spasticity (Siddall *et al.* 2003; Wrigley *et al.* 2009). Therefore, a deep and fine scale understanding of the complexity of CoRe is still needed to improve our knowledge of the plastic process in order to find new strategies to modulate the strength of the reorganization and to improve functional recovery.

Over the past two decades, the use of large-scale experimental approaches such as extracranial electroencephalographic recordings (Green *et al.* 1998), voltage sensitive dyes (Ghosh *et al.* 2010) and functional magnetic resonance imaging (Endo *et al.* 2007) has revealed important insights about the process of CoRe in the time period ranging from days to months after the injury. In addition, fine-scale techniques using *in vivo* electrophysiological recordings demonstrate increased neuronal activity in the deafferented cortex in response to peripheral stimulation of body regions located above lesion level (Jain *et al.* 1998, 2008). Interestingly, changes in the cortical activity after SCI have been mostly studied by using electrophysiological recordings from layer 5 neurons (Aguilar *et al.* 2010; Ghosh *et al.* 2012; Ganzer *et al.* 2013; Humanes-Valera *et al.* 2013; Humanes-Valera *et al.* 2017; Manohar *et al.* 2017). Important reasons support this selection: layer 5 pyramidal neurons receive

direct thalamic inputs that are reduced after SCI; its apical dendrite spans multiple layers to integrate inputs along the vertical column axis; layer 5 corticospinal neurons are directly axotomized after a SCI, thereby altering the columnar spontaneous activity; and finally it is the main cortical output to control behaviour and sensory ascending inputs (Canedo & Aguilar 2000; Manohar *et al.* 2017; Larkum *et al.* 2018). In this regard, SCI has been described as: (1) altering the neuronal excitability at both thalamic level and cortical layer 5 activity (Jain *et al.* 2008; Liang & Mendell 2013; Alonso-Calviño *et al.* 2016), (2) inducing spine loss in the proximal segments of the apical dendrite of axotomized and non-axotomized corticospinal layer 5 neurons in the deafferented cortex (Ghosh *et al.* 2012), and (3) increasing the strength of corticocortical connections (Endo *et al.* 2007; Ganzer *et al.* 2013; Humanes-Valera *et al.* 2017; Manohar 2017). However, the neocortex is a complex structure composed of six horizontal layers that are spatially and functionally defined by vertical columns. Each layer is defined by different functional properties, cellular composition, and input/output from and to cortical and subcortical regions that under physiological conditions work together to generate and control the pattern of cortical activity. Therefore, the effects that a SCI will produce at the cortical level might not be restricted to layer 5 but might span different cortical layers as a result of altered input statistics that take into account changes in the spontaneous excitability, altered retrograde messaging due to the axotomy, and changes in thalamic and cortical connectivity. In this study, we determine whether each cortical layer may reflect different aspects of CoRe after SCI based in the local network, columnar connections and corticocortical connections, in addition to a direct effect on layer 5 pyramidal neurons.

Functional imaging and electrophysiological studies have revealed that CoRe is a physiological phenomenon in which the time elapsed after the injury may be considered a key factor. In this regard, functional changes have been observed immediately after SCI in different animal models as rodents (Aguilar *et al.* 2010; Yagüe *et al.* 2011, 2014; Humanes-Valera *et al.* 2013) and pigs (Jutzeler *et al.* 2018).

**Marta Zaforas** is a PhD candidate in Neuroscience at the Hospital Nacional de Parapléjicos, Toledo, Spain. She obtained her bachelor's degree in Biology and master's degree in Neuroscience and Behavioural Biology. Her PhD research is focused on the cortical layer contribution to circuit reorganization after spinal cord injury. She is interested in how the units of cortical circuits process sensory information and how the disruption of their communication leads to a development-like plastic environment. **Juliana M. Rosa** has developed her scientific career studying the mechanisms by which neural circuits process sensory information with an emphasis on synapses and the neuron–glia network, first with Dr Leon Lagnado (Cambridge, UK) and later with Dr Marla Feller (Berkeley, USA). In 2019 she became a Principal Investigator at the Hospital Nacional de Parapléjicos, starting her own group in 2020 focused on the restoration of neural circuit functions after CNS injuries by targeting glial cell types.



Previous data from our group show that, a few minutes after the injury, both intact and deprived somatosensory cortex became more responsive to peripheral sensory stimulation above the lesion level (Humanes-Valera *et al.* 2013; Yagüe *et al.* 2014) and spontaneous activity is drastically reduced (Aguilar *et al.* 2010; Fernández-López *et al.* 2019). In addition to the cortical changes, SCI also modifies thalamic and brainstem spontaneous and evoked neuronal excitability, which may be linked to the changes observed in the somatosensory cortex (Jain *et al.* 2008; Alonso-Calviño *et al.* 2016). Therefore, for a precise understanding of the physiological basis of CoRe initiation across cortical layers in deafferented cortex, here we used an acute model of SCI in which simultaneous electrophysiological recordings from six cortical layers were obtained. For this purpose, the use of a vertical array spanning the full cortical depth allows us to determine how SCI affects the neuronal activity within individual layers, the vertical relationship between layers, as well as horizontal connections from adjacent intact cortical columns.

Using *in vivo* electrophysiological recordings from anaesthetized rats, we studied how neuronal activity mediated by corticocortical and thalamic connections as well as the local circuitry in the hindlimb cortex (HLCx) is immediately affected by deafferentation after a thoracic SCI. For this, we used a vertical multielectrode array to determine the neuronal excitability across layers of the deprived HLCx during evoked and spontaneous activity. Peripheral stimulation of the contralateral forelimb showed a layer-dependent increase in sensory-evoked local field potential (LFP) responses across HLCx layers indicating that changes in neuronal network properties of the deprived cortical column may favour excitability. However, a striking heterogeneity was observed when other physiological parameters were analysed. Infragranular L5/6, but not L2/3, exhibited increased LFP slope, increased multiunit activity and delayed onset latencies. Contrary to evoked responses, spontaneous activity was mostly affected in supragranular layers as observed by increased high rhythm frequencies and probability of initiating up-states. Altogether, our data indicate that SCI immediately modifies the local circuitry within the deprived cortex allowing supragranular layers to better integrate spontaneous cortico-cortical information, thus modifying the excitability of the column, and infragranular layers to better integrate evoked sensory inputs to preserve subcortical outputs.

## Methods

### Ethical approval

Experiments were performed on two groups of male Wistar rats of age 2–6 months, mean weight 395 (SD 45) g.

Group 1 was intended for the cortical layer study ( $n = 29$ , Ctr:WI Charles River, Barcelona, RRID:RGD\_737929); and group 2 was intended for the thalamo-cortical study ( $n = 7$ ; Ctr:WI Charles-River RRID:RGD\_737929). All animals were housed two per cage in standardized cages, with *ad libitum* access to food and water and maintained at 23°C on a 12-h light/dark cycle. All steps of the experimental procedure were performed in such a way to minimize the animals' pain and suffering and were approved by the Ethical Committee for Animal Research at the Hospital Nacional de Paraplégicos (reference number for group 1: 152CEEA/2016; group 2: 85CEEA/2012). Note that in group 2, the cortical dataset used in the present work was obtained simultaneously with the dataset regarding the thalamic activity after SCI that has been previously published in Alonso-Calviño *et al.* (2016). However, the cortical dataset has been analysed for the first time for the present work, in line with the rule of three Rs in order to reduce the number of experimental animals. Approximately 14% of the total number of animals died before or during the experimental procedure for SCI, due to anaesthesia intolerance (Field *et al.* 1993). All researchers involved in the study were aware of the ethical principles under which *The Journal* operates and complied with the animals' ethics checklist set out by *The Journal of Physiology*, the International Council for Laboratory Animal Science, the European Union 2010/63/EU and the ARRIVE guidelines.

### Experimental approach

The general experimental approach (anaesthesia, surgery and peripheral stimulation) was similar to that used in our previous studies (Aguilar *et al.* 2010; Humanes-Valera *et al.* 2013; Alonso-Calviño *et al.* 2016; Humanes-Valera *et al.* 2017). Briefly, animals were anaesthetized with an intraperitoneal injection of urethane (1.5 g/kg i.p., Sigma-Aldrich, Spain, U2500-100G), placed in a stereotaxic frame (SR-6 Narishige Scientific Instruments, Tokyo, Japan) passively ventilated at 2 litres O<sub>2</sub>/min by a mask (Medical Supplies & Services, Int. Ltd, Keighley, UK) and body temperature kept constant at 36.5°C using a homeothermic blanket (Cibertec SL, Madrid, Spain). The optimal level of anaesthesia was settled at stage III-4 of cortical activity described by Friedberg *et al.* (1999). The absence of reflexes to forelimb stimuli, spontaneous whisker movements and corneal reflex was also used to verify the level of anaesthesia. Constant verification of EEG activity and reflexes took place throughout the experiment to guarantee the optimal level of anaesthesia. Then, lidocaine 5% (Normon, Madrid, cat. no. P06B1) was applied subcutaneously into the areas of the incision, and thoracic laminectomy (at T9–T10 vertebra) was performed keeping the dura mater intact and protected

until the moment of performing a complete transection of the spinal cord. Next, the skull was exposed, and a craniotomy was performed on the right hemisphere over the hindlimb representation of the primary somatosensory cortex (AP 0 to  $-3$  mm; ML 1 to 4 mm; Paxinos & Watson, 2007) to allow the lowering of a vertical array for further recording of neuronal activity. The stability of recordings was improved by drainage of the cisterna magna and covering the exposed cortex with agar at 4% (Sigma-Aldrich, cat. no. A7002-250G). The exact location of the probe was optimized by assessing the responses to tactile stimulation of the rat's hindlimb with a cotton swab while listening to the recorded signal through a pair of loudspeakers.

### Electrophysiological recordings and peripheral stimulation

Extracellular recordings were obtained from 24 rats by a linear vertical probe of 32 iridium contacts of  $177 \mu\text{m}^2$  spaced at  $50 \mu\text{m}$  (impedance  $1\text{--}4 \text{ M}\Omega$  at  $1 \text{ kHz}$ ; ref. A1X32-6mm-50-177-A32, NeuroNexus Technologies Inc., Ann Arbor, MI, USA). The array was slowly introduced ( $1\text{--}2 \mu\text{m/s}$ ; Fiáth *et al.* 2019) through the craniotomy into the HLCx and a ground electrode was placed in the parietal muscular tissue. The reference electrode was built in the vertical probe,  $0.5 \text{ mm}$  above the superficial recording site and outside the cortex (area  $4200 \mu\text{m}^2$ ). The recording protocol started  $\sim 40 \text{ min}$  after the end of the electrode insertion to allow recovery of cortical tissue following the time line in Fig. 1A. Spontaneous activity was recorded during  $10 \text{ min}$ . The stimulation protocol ( $0.5 \text{ ms}$  duration at  $0.5 \text{ Hz}$ ) was applied through bipolar needle electrodes ( $30\text{G}$ , B. Braun, Melsungen, Germany) located subcutaneously in the wrist of contralateral forelimb and hindlimb extremities. Two different intensities were applied: (1) low intensity ( $0.5 \text{ mA}$ ) to activate only a fraction of the available peripheral fibres, mainly low-threshold primary fibres running through the lemniscal pathway from the dorsal column to the brainstem, and (2) high intensity ( $5 \text{ mA}$ ) to activate the maximum number of fibres including high-threshold primary fibres that synapse in the dorsal horns of the spinal cord including the spinothalamic tract (Lilja *et al.* 2006; Yague *et al.* 2011). However, note that all data analysed throughout this study were obtained from responses showing an initial latency below  $15 \text{ ms}$ , which corresponds to low-threshold peripheral fibres (tactile and proprioceptive) from the entire paw (digits and palm). After recordings of evoked and spontaneous activity in control conditions, complete transection of the spinal cord was performed using spring scissors. Immediately after transection, pulses of  $10 \text{ mA}$  electrical stimulation were applied to the contralateral

hindlimb to confirm that no physiological responses were evoked by stimuli delivered below the level of the lesion. Complete spinal cord transection was also visually confirmed under the surgical microscope by the total separation of the borders with the help of a small piece of an absorbable haemostatic gelatin sponge (Spongostan, Ferrosan Medical Devices, Denmark). Recordings were continuously acquired during the transection to confirm the stability of the recordings. Approximately  $20\text{--}30 \text{ min}$  after the transection, the same protocol as before SCI was applied. All recording data were converted into digital data at a  $40 \text{ kHz}$  sampling rate ( $16/24$  rats) and  $1 \text{ kHz}$  ( $8/24$  rats), with 16-bit quantization by an OmniPlex System controlled by OmniPlex Software (RRID:SCR\_014803, Plexon Inc., Dallas, TX, USA). All the  $40 \text{ kHz}$  signals were offline-filtered into two signals: LFP (low-frequency band: up to  $1 \text{ kHz}$ ) and multiunit activity (MUA; finite impulse response (FIR) bandpass:  $0.3\text{--}3 \text{ kHz}$ , gap  $0.12 \text{ kHz}$ ) by using Spike2.v7 (RRID:SCR\_000903, Cambridge Electronic Design (CED), Cambridge, UK).

Once the experimental protocol for electrophysiological recordings was completed, animals were prepared for transcardial perfusion to preserve the brain tissue, which was submitted to posterior histological procedures (see 'Histology' section). For this purpose, an overdose of anaesthetic (urethane  $1.5 \text{ g/kg}$  i.p., Sigma-Aldrich, U2500-100G) was applied to induce anaesthetic level IV (Friedberg *et al.* 1999), which was confirmed by a flat EEG, while heart beating and respiration were optimally preserved.

### Histology

At the end of the experiments and after receiving an overdose of urethane ( $1.5 \text{ g/kg}$ ) as described above, animals were transcardially perfused with heparinized saline followed by 4% paraformaldehyde. Then the brain was removed and post-fixed in the same fixative solution for  $24 \text{ h}$  at  $4^\circ\text{C}$ . After fixation, brain tissue was cryopreserved in a 30% sucrose solution until it sank and coronal sections at  $50 \mu\text{m}$  thickness were obtained with a sliding microtome (Microm HM 450 V; Microm International GmbH, Dreieich, Germany). Following washing in  $0.1 \text{ M}$  phosphate buffer, sections were mounted on gelatin slides, air-dried, processed for tioneine (Nissl) staining (T7029-5G, Sigma-Aldrich), dehydrated in xylene and coverslipped with DePeX (cat. no. 18243.01, SEVA, Heidelberg, Germany).

### Thalamocortical recordings and analysis

Simultaneous electrophysiological recordings from forelimb cortex (FLCx) and HLCx in response to peripheral forelimb stimulation were obtained by using two

single tungsten electrodes located on infragranular layer 5 of both cortical regions under control conditions and after SCI. Note that this dataset was obtained simultaneously to the thalamic data previously published in Alonso-Calviño *et al.* (2016), but the cortical dataset has been for the first time analysed for the present work. Experimental protocol was the same as for experiments described above. Briefly, experiments were performed on male Wistar rats ( $n = 7$ , Ctr:WI Charles River RRID:RGD\_737929) aging 2–6 months. Animals were housed two per cage in standardized cages, with *ad libitum* access to food and water and maintained at 23°C on a 12-h light/dark cycle. All experiments were performed in accordance with the International Council for Laboratory Animal Science and the European Union 2010/63/EU and were approved by the Ethical Committee for Animal Research at the Hospital Nacional de Paraplégicos (85/2012) and funded by Spanish Ministry of Economy and Competitiveness and co-funded by FEDER (SAF2012-40109).

Extracellular recordings were obtained using tungsten electrodes (TM31C40KT, 4 M $\Omega$  impedance at 1 kHz or TM31A50KT, 5 M $\Omega$  impedance at 1 kHz; World Precision Instruments Inc., Sarasota FL, USA). All recordings were pre-amplified in the DC mode, low pass filtered (<3 kHz) and amplified using a modular system (Neurolog, Digitimer Ltd, Welwyn Garden City, UK). Analog signals were converted into digital data at a 20 kHz with 16-bit quantization via CED Power 1401 apparatus (RRID:SCR\_017282) controlled by Spike2. The data were analysed using Spike2 software. Onset latency of cortical responses was obtained using the same method as for the HLCx multielectrode recordings phase (Fedchyshyn & Wang 2007). In order to obtain comparable data, animals used for this analysis presented a deep state of anaesthesia (III-4; Friedberg *et al.* 1999; Erchova *et al.* 2002) corresponding to slow-wave cortical activity, and evoked cortical responses to peripheral forelimb stimulation were used at 5 mA (0.5 Hz).

Once the experimental protocol for electrophysiological recordings was completed, animals were prepared for transcardial perfusion to preserve the brain tissue with an overdose of anaesthetic (urethane 1.5 g/kg i.p., Sigma-Aldrich, U2500-100G) applied to induce anaesthetic level IV (Friedberg *et al.* 1999), which was confirmed by a flat EEG, while heart beat and respiration were optimally preserved.

### Data analysis: evoked responses and spontaneous activity

For laminar profile analysis, LFP-evoked responses from each electrode were averaged across 100 stimuli (0.5 Hz)

and measured as the maximum amplitude to negative peak (mV) in the local fast response in a time window corresponding to 5–60 ms or 5–30 ms following sensory stimulation of hindlimb or forelimb, respectively. In order to quantify MUA, local field potentials were band-pass filtered (FIR bandpass 0.3–3 kHz, gap 0.12 kHz) to obtain multi-unit activity. MUA was then rectified (rMUA), downsampled to 2 kHz and averaged across 100 stimuli to measure the total voltage resulting from the averaged area of responses ( $\mu$ V). The background voltage corresponding to basal activity was subtracted from response voltage (equal time to analysis window but preceding stimulus). For layer analysis, electrode sites were grouped according to layer thickness following these depths: layer 2/3 (150–650  $\mu$ m), layer 4 (700–1000  $\mu$ m), layer 5 (1050–1450  $\mu$ m) and layer 6 (1500–2000  $\mu$ m; Fiáth *et al.* 2016). For LFP data analysis, electrode measures were averaged across layers while neuronal signals obtained from individual channels (rMUA) were summed within a layer to allow robust detection of the neuronal activity.

Onset latency of evoked LFP and rMUA was calculated for each layer by fitting the averaged response with an equation of the form of the Boltzmann charge–voltage function. This equation was solved for its fourth derivative giving a highly accurate measure of the response onset independent of the slope rise phase (Fedchyshyn & Wang 2007). Slopes were measured by using the formula  $\Delta V/(t_1 - t_2)$ , where  $\Delta V$  is the LFP amplitude,  $t_1$  is the onset and  $t_2$  is the time of the negative peak. For analysis of the spontaneous cortical activity, up-states within the slow-wave activity (SWA) were first analysed in periods of 5 min of spontaneous HLCx recordings for each subject to compare cortical state immediately before and between 10 and 30 min after SCI. Raw signals were downsampled to 500 Hz and then a fast Fourier transform analysis was performed to confirm that the maximum peak frequency of the recordings was below 1 Hz. Frequency power (mV<sup>2</sup>) was extracted for each electrode by summing power within same frequency band: SWA (0.1–1 Hz), delta (1–4 Hz), theta (4–8 Hz), alpha (8–12 Hz), beta (12–25 Hz), low gamma (25–50 Hz) and high gamma (50–80 Hz). LFP power obtained from individual electrodes within a layer was averaged to obtain a layer frequency power. Finally, the power of each frequency band was normalized to the total power of the LFP recording (0.1–80 Hz) to obtain the relative power of each band. Additionally, individual up-states were selected within periods of 60 s of LFP for each subject to obtain the onset in control and acute SCI using the same methodology as for the onset of evoked-LFP responses (Fedchyshyn & Wang 2007). To calculate the velocity of propagation, the electrode presenting the earliest onset was taken as reference, and the velocity rate calculated

as the distance in the cortical depth as a function of time.

### Statistical analysis

Statistical analyses were performed using Statistica.Ink (RRID:SCR\_014213, Statsoft Ibérica, Lisbon, Portugal). The Shapiro–Wilk test was used to test normality of the distribution ( $P > 0.05$ ). If normality was violated (non-Gaussian distribution  $P < 0.05$ , rMUA response magnitude, Fig. 3), data were transformed to a normal distribution by using the square root. Grubb's test was used to identify and remove outliers ( $\alpha = 0.05$ ). Our main hypothesis (differences across layers) was first tested in our control data set (pre-lesion) using one-way analysis of variance (ANOVA) with Layer as the independent factor. Dependent differences between pre- and post-injury among animals and layers were determined by two-way ANOVA, with Layer as an independent factor and Time as a repeated measures factor (two levels, Pre- and Post-lesion). When significant differences in analysis of variance were found, groups were further compared using Tukey's *post hoc* test. For statistical analysis of the dual recording site from intact and deafferented cortices (Fig. 6), we used a two-tailed paired Student's *t*-test with a Bonferroni correction for multiple comparisons ( $P < 0.025$ ). The threshold for statistical significance was  $P < 0.05$  throughout. Group measurements are expressed as means  $\pm$  standard deviation (SD). Graphs and figures were made using IgorPro (WaveMetrics, Lake Oswego, OR, USA, RRID:SCR\_000325) and Adobe Illustrator (RRID: SCR\_010279).

## Results

### Laminar analysis of evoked neuronal responses in the somatosensory cortex following peripheral stimulation

We first characterized the evoked local field potentials (evoked LFP) across layers of the HLCx in response to sensory stimulation delivered either to the contralateral hindlimb (HL) or to the forelimb (FL) in intact anaesthetized animals (Fig. 1). For that, we used a linear 32-multielectrode probe inserted vertically into the HLCx such that recording sites were located across all layers in a single column to simultaneously record LFPs and local multiunit activity (MUA). Figure 1A shows a schematic representation of the recording location and stimulation protocol as well as a histological preparation showing an electrode track into HLCx (Fig. 1B). Representative examples of averaged evoked LFPs across the entire depth of HLCx in response to a 5 mA hindlimb stimulation (0.5 Hz) are shown in the left panel of Fig. 1C. Note

that high intensity stimulation was chosen to maximize the activation of peripheral nerves to ensure the full engagement of cortical circuits involved in somatosensory processing (Lilja *et al.* 2006). The laminar profile of averaged LFP responses of the population obtained by hindlimb stimulation showed a clear difference in the response magnitude across the cortical depth, with a maximum peak at distances from surface between 700 and 1000  $\mu\text{m}$  corresponding to the thalamorecipient granular layer 4. No differences were observed using low intensity stimulation, which resembles light mechanical stimuli that preferentially activate dorsal column pathways (Lilja *et al.* 2006). Current source density (CSD) analysis was overlapped to LFP traces to determine the entrance of synaptic inputs in different cortical layers (Fig. 1C, heat map) showing an evident current sink (inward current) in L4. The active sink was surrounded by two strong current sources (outward current), one short-lasting in L2/3 and another long-lasting in the infragranular layers (L5 and L6). A small and elongated current sink was also observed in L6, which may refer to the thalamocortical loop initiated by evoked responses. The greater LFP response magnitude and the current sink at the thalamorecipient L4 corroborate the correct location of the electrode at the somatotopic representation of hindlimbs. Finally, MUA responses (Fig. 1D, left panel) were analysed by rectifying the neuronal firing (rMUA) obtained in response to peripheral stimulation at high and low intensities (Fig. 1D, right panel). The area of the evoked rMUA showed robust neuronal firing in the upper infragranular layer (i.e. L5), while L2/3 and L6 neurons showed a low firing response. A similar laminar profile of neuronal responses was observed using low intensity stimulation (0.5 mA). The sparse and low firing observed in L2/3 under our experimental condition corroborates previous studies using distinct techniques such as *in vivo* and *in vitro* patch clamp, intracellular recordings (Wilent & Contreras, 2004; Jacob *et al.* 2017) and *in vivo* live  $\text{Ca}^{2+}$  imaging (Clancy *et al.* 2015).

We next examined the pattern of cortical responses when the peripheral stimulation was applied to an adjacent, non-corresponding somatotopic body region, i.e. recording in HLCx, while stimulating forelimb afferents. Figure 1E shows LFP representative traces produced in the HLCx in response to high intensity electrical stimulation of the contralateral forelimb. Despite the small amplitude, evoked LFP responses were clearly observed across all recording channels with infragranular layers showing the highest magnitude. In addition, current sinks representing the synaptic inputs from FLCx were visible in L2/3 and L5. Similar results were also observed using 0.5 mA stimulation indicating a strong HL–FL cortical connectivity even to low intensity stimuli. In response to high stimulation, rMUA in infragranular layers showed a clear evoked activity with a peak in L6,

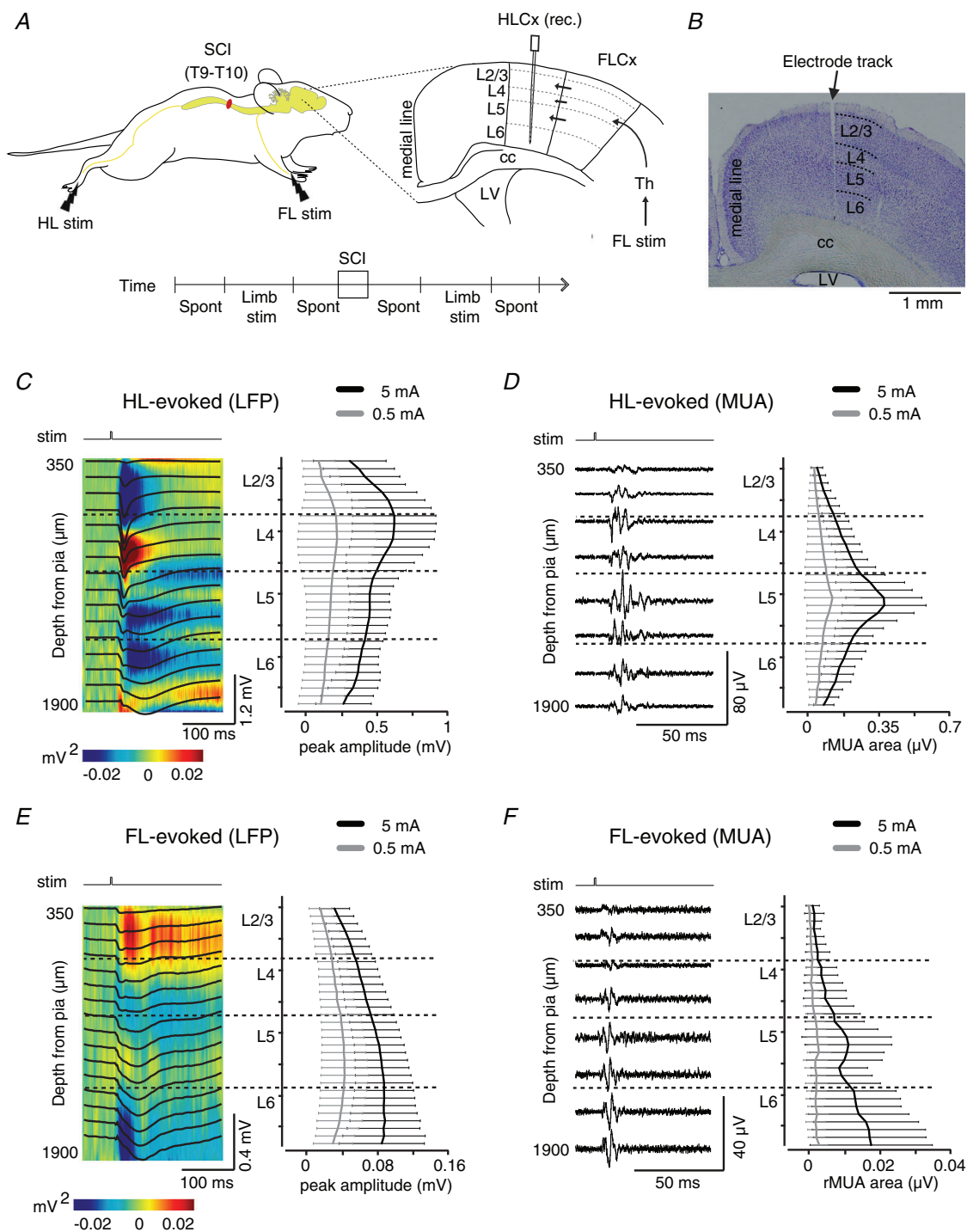


**Figure 1. Experimental approach and laminar characterization of evoked sensory responses in hindlimb cortex**

A, schematic illustration of the experimental protocol. Extracellular recordings were obtained using a multielectrode probe inserted in the hindlimb of the primary somatosensory cortex (HLCx) from anaesthetized rats. Complete transection of the spinal cord was performed at thoracic level (SCI, T9–T10). Spontaneous activity (Spont) and evoked responses to electrical stimulation at high (5 mA) and low (0.5 mA) intensity delivered to the contralateral hindlimb (HL stim) and forelimb (FL stim) were recorded following the described timeline in control conditions and immediately after SCI. In the cortical representation, black arrows crossing cortical regions indicate corticocortical

connections and thalamic inputs into FL cortex in response to forelimb stimulation (FL stim). Cortical layers were designated as L2/3, L4, L5 and L6. cc, corpus callosum; LV, lateral ventricle; Th, thalamus. *B*, Nissl-stained coronal section of a representative rat showing an electrode track in HLCx (white line crossing all layers of the HLCx). Dotted lines indicate the limits of each cortical layer. *C*, left, continuous black traces represent sensory-evoked LFP across HL cortical layers in response to a 5 mA electrical stimulation of the contralateral hindlimb (HL). Recordings obtained every 100  $\mu\text{m}$  were plotted on top of the current source density (CSD) map from the same recordings. Colour map represents the CSD contour plot obtained from the same LFP recording shown in the graph. Right, averaged evoked LFP amplitudes from each electrode of the array as a function of cortical depth in response to low (0.5 mA, grey) and high (5 mA, black) sensory stimulation. *D*, left, filtered LFP traces from the same recordings in *C* showing evoked MUA signal from representative electrodes. Right, averaged area of rectified MUA (rMUA) from the same population in *C*. *E*, left, representative traces of evoked LFP overlapped on the CSD map in response to 5 mA FL stim from the same animal as *C* and *D*. Note that in this case current sinks are stronger in L2/3 and L5. Right, averaged evoked LFP amplitudes as a function of cortical depth in response to low (0.5 mA, grey) and high (5 mA, black) FL stim. *F*, left, filtered LFP traces from the same recordings as in *E* (left) showing the evoked MUA signal. Right, averaged area of rMUA from the same population in *E*. Horizontal dashed lines indicate layer boundaries. Graphs represent means  $\pm$  SD ( $n = 24$  rats). See Table 1 for statistical details. [Colour figure can be viewed at [wileyonlinelibrary.com](http://wileyonlinelibrary.com)]

while L2/3 and L4 exhibited only sparse and very low response (Fig. 1*F*). Therefore, our data indicate that each cortical layer exhibits a characteristic neuronal activity in response to stimulation of its own receptive field as shown in previous studies (Wilent & Contreras, 2004; Sakata & Harris, 2009), but also in response to non-preferential peripheral stimulation (i.e. neuronal activity in HLCx in response to forelimb stimulation), which evidences a heterogenic cortical excitability probably due to the composition of each local circuit and synaptic inputs. Statistical analysis comparing the response magnitude

of cortical layers for each condition is summarized in Table 1.

### Recording stability during the full transection of the spinal cord

We next sought to determine the effects that an immediate SCI had on the neuronal excitability of the deprived neurons across all cortical layers. As a first approach, we recorded the stability of our recordings during the

**Table 1. Related to Fig. 1, evoked LFP and rMUA recorded in HLCx in response to either hindlimb or forelimb stimulation**

	Limb stimulated	Intensity (mA)	Layer effect	Post-hoc Tukey ( $P < 0.05$ )	
LFP amplitude (mV)	HL	0.5	$F_{(3,89)} = 0.9$ $P = 0.4639$		
		5	$F_{(3,89)} = 6.7$ $P = 0.0004$	L2/3 vs. L6; $P = 0.0485$ L4 vs. L6; $P = 0.0003$	
	FL	0.5	$F_{(3,92)} = 4.1$ $P = 0.0087$	L2/3 vs. L5; $P = 0.0072$ L2/3 vs. L6; $P = 0.0454$	
		5	$F_{(3,92)} = 12.1$ $P < 0.0001$	L2/3 vs. L5; $P = 0.0002$ L2/3 vs. L6; $P = 0.0002$ L4 vs. L6; $P = 0.0243$	
	rMUA area ( $\mu\text{V}$ )	HL	0.5	$F_{(3,60)} = 2.6$ $P = 0.0617$	
			5	$F_{(3,60)} = 26$ $P < 0.0001$	L2/3 vs. L4; $P = 0.0010$ L2/3 vs. L5; $P = 0.0002$ L2/3 vs. L6; $P = 0.0053$ L4 vs. L5; $P = 0.0002$ L5 vs. L6; $P = 0.0002$
FL		0.5	$F_{(3,60)} = 6.2$ $P = 0.0010$	L2/3 vs. L5; $P = 0.004$ L2/3 vs. L6; $P = 0.033$ L4 vs. L5; $P = 0.014$	
		5	$F_{(3,60)} = 9.5$ $P < 0.0001$	L2/3 vs. L5; $P = 0.0016$ L2/3 vs. L6; $P = 0.0003$ L4 vs. L5; $P = 0.0258$ L4 vs. L6; $P = 0.0048$	

One-way ANOVA for control responses ( $n = 24$  rats). Tukey *post hoc* comparisons are shown for significances  $P < 0.05$ .

exact moment of the spinal transection. Figure 2A shows original recordings of selected channels from an array of 32 electrodes inserted on the hindlimb cortex while applying 0.5 Hz electrical stimulation on the contralateral hindlimb. Before SCI, all layers exhibited slow-wave oscillations composed of up (periods of synchronized activity) and down (periods of neuronal silence) states that emerge as a consequence of anaesthesia or the sleep condition. On top of the slow-wave activity, fast and enlarged evoked synaptic responses are evidenced in response to peripheral sensory stimulation. While performing the recordings (and without removing the electrode from the hindlimb cortex), we proceeded with the full transection of the spinal cord. During the injury, the slow-wave activity is disrupted by only a few seconds as observed by the sustained depolarization observed across all layers of the deprived cortex (shaded area in Fig. 2B). After this short period of time,

cortical activity from hindlimb neurons returned to the previous slow-wave oscillations, while evoked sensory responses were abolished, confirming the full transection of the spinal cord. The same pattern of short 'synaptic barrage' was also observed when obtaining simultaneously extracellular recordings from layer 5 neurons of the intact forelimb cortex and intracellular recordings from layer 5 neurons in the hindlimb cortex (Fig. 2C). The intracellular recording of the layer 5 pyramidal neuron shows that the membrane potential and spontaneous activity were only disrupted by a sustained depolarization with only a few action potentials during the transection, and that the membrane potential immediately returned to baseline after this short period (Fig. 2C, black traces, intracellular S1HL). In parallel, the extracellular forelimb cortical recordings (Fig. 2C, green traces S1FL MUA) show parallel changes of activity, but it must be noted that the forelimb cortex is neither directly

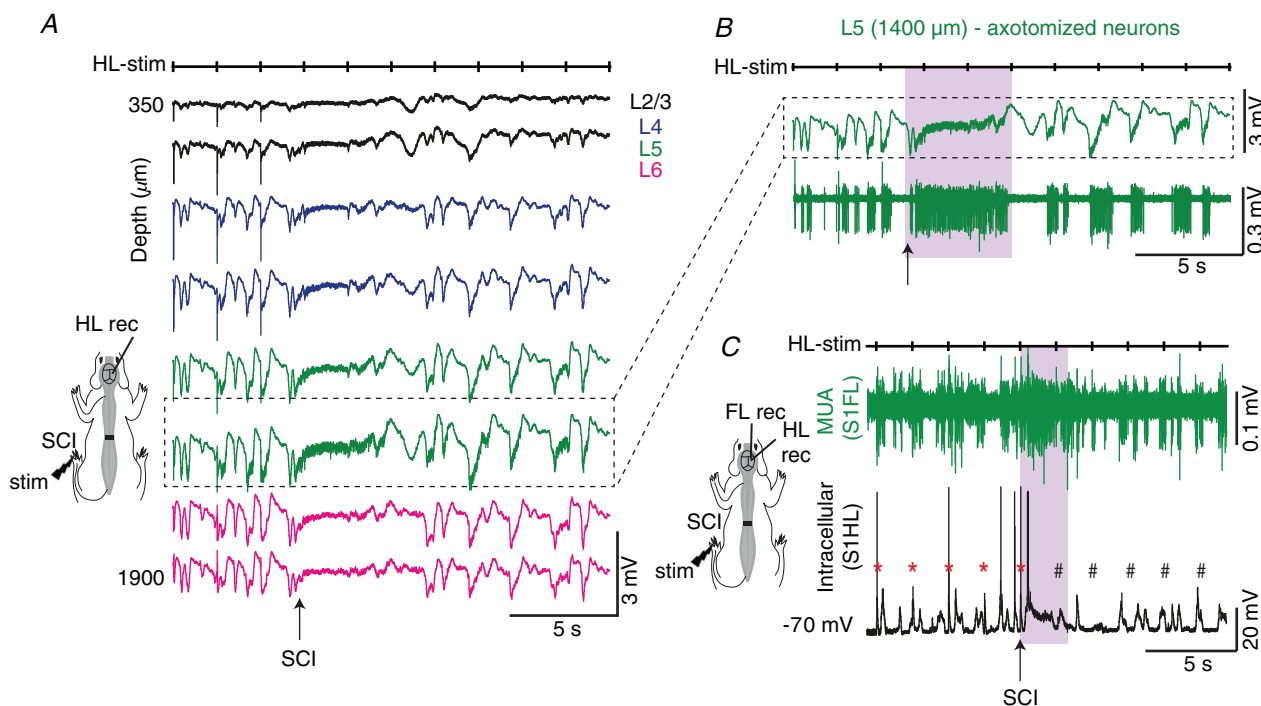


### Figure 2. Stability of cortical recordings during spinal cord injury

A, original spontaneous LFP recordings obtained from distinct layers of hindlimb cortical location before SCI, during the moment of SCI (marked by an arrow) and immediately after SCI. Note that SCI triggers a transient (<5 s) increase of activity that could be associated to a 'cortical barrage'. B, raw LFP recording from layer 5 (top) and extracellular action potentials observed after band-pass filtering (0.3–3 kHz) (bottom). Note that the immediate effect of SCI on cortical layer 5 is observed as a transient (<5 s) increase in the neuronal excitability (shaded area) that is shortly re-synchronized to produce the characteristic SWA oscillations of up-states and down-states. C, extracellular recording from intact forelimb (layer 5) somatosensory cortex (S1FL; green traces correspond to bandpass-filtered MUA) obtained simultaneously with an intracellular recording from a S1HL layer 5 neuron (black traces). Arrows indicate the moment of full transection of the spinal cord. Note that synaptic depolarization (<5 s) after SCI is observed in both intact (S1FL) and deafferented (S1HL) cortices. Note in A–C the inclusion of an upper trace named HL-Stim, indicating the 5 mA hindlimb stimulation (0.5 Hz) used throughout the recording to confirm the full transection of the spinal cord. Before SCI, HL-stim evoked LFP and action potentials in both extracellular (fast negative deflections in A and B) and intracellular recordings (red asterisks in C) which was abolished after full transection of the spinal cord (black hashes in C). [Colour figure can be viewed at [wileyonlinelibrary.com](http://wileyonlinelibrary.com)]

damaged nor sensory deprived by a thoracic SCI. The latter confirms previous findings from our group showing that SCI affects brain states in both deprived and intact areas (Aguilar *et al.* 2010; Humanes-Valera *et al.* 2013). Therefore, these experiments demonstrated the neuronal stability of our recordings and the complete transection of the spinal cord.

### SCI induces layer-dependent functional changes in the sensory deprived cortex

Given the layer-specific activity induced in the HLCx in response to forelimb stimulation under control conditions, we hypothesized that SCI should induce specific effects on the evoked LFP in a layer-dependent manner. To explore this, we investigated the neuronal activity across cortical layers immediately after sensory deprivation due to SCI in 24 rats (Fig. 3). As expected, abolition of the evoked LFP was immediately observed in all layers of the HLCx in response to hindlimb stimulation, confirming the complete loss of sensory inputs (Fig. 3A). When 5 mA peripheral stimulation was applied to the contralateral forelimb, the magnitude of evoked LFP produced in HLCx was significantly increased in all layers but L6 (Fig. 3B, two-way repeated measures ANOVA, SCI  $F_{(1,91)} = 50.2$ ,  $P < 0.0001$ ), indicating heterogeneous immediate changes in the excitatory post-synaptic activity of local pyramidal neurons and/or in the strength of arriving synaptic inputs. Next, we examined the area of the rectified MUA (rMUA) as a measure of the local neuronal activity in each cortical layer recorded in a subset of SCI animals (19 out of 24 SCI animals; Fig. 3C). Figure 3D shows examples of evoked rMUA from each channel superimposed on a colour-coded map from the same animal in response to high intensity stimulation (5 mA) before and after SCI. Two-way repeated measures ANOVA showed differences for layers ( $F_{(3,60)} = 12.5$ ,  $P < 0.0001$ ) and SCI condition ( $F_{(1,60)} = 18.1$ ,  $P < 0.0001$ ), but no interaction between layers and SCI ( $F_{(3,59)} = 1.2$ ,  $P = 0.3145$ ). Before SCI, L2/3 and L4 neurons exhibited very low activity, while robust firing was observed only in L5 and L6 in response to forelimb stimulation. After SCI, neuronal firing tended to increase in all layers (see original traces in Fig. 3E), with L5 rMUA significantly increased post-lesion ( $P = 0.0378$ ). These results demonstrate that immediate sensory deprivation due to SCI produces increased neuronal firing in infragranular layers, and importantly creates differences in neuronal excitability among cortical layers of the deprived HLCx. Due to the non-consistent responses obtained among individuals when low intensity stimulation was applied, herein data were considered only for responses obtained to high intensity stimulation in forelimb (5 mA).

Next, we explored whether cortical deafferentation would affect individuals non-uniformly, and more specifically that a subset of our experimental animals may not exhibit the overall changes in the neuronal cortical activity following immediate SCI. To explore whether this assumption was true, we plotted the individual values corresponding to the ratios between the evoked LFP response post- and pre-SCI obtained from layer 5 neurons for each studied animal (Fig. 3F). Note that layer 5 was chosen due to the large responses following forelimb stimulation and the significant effect previously described after SCI (Humanes-Valera *et al.* 2017; Fernández-López *et al.* 2019). This allowed us to identify a clear separation of animals in which SCI induced increments in the magnitude of the evoked LFP (ratio  $>1$ , 19/24 animals, 79%), from those animals in which LFP amplitude remained stable or even decreased with a ratio  $<1$  (5/24 animals, 21%; Fig. 3F). Therefore, our results strongly suggest that SCI immediately increases the excitability of deprived neurons in a layer-specific manner. Moreover, we observed that immediate cortical deprivation does not affect homogeneously all subjects of a population that could be clustered in affected and non-affected subsets.

### SCI strongly affects the corticocortical and thalamocortical connectivity between infragranular layers

Next, we sought a deep characterization of the functional alterations produced in the deafferented HLCx in response to forelimb stimulation in both groups of animals. It has been proposed that increased cortical responses after SCI could be mediated by a reduction of inhibitory activity that consequently unmasks latent excitatory inputs of deafferented region, thereby modulating the dynamics of local responses (Sydekum *et al.* 2014). Taking this assumption into account, our proposed hypothesis was that sensory deprivation would differentially affect the kinetics of LFP produced at each cortical layer based on the different inhibitory tone relieved at the local neuronal network. Thus, we first analysed the slope values (decay rate in mV/s) of evoked LFP that are often used to determine changes in the arrival and/or synchronization of synaptic inputs and are usually affected by changes in the excitation–inhibition balance (Fig. 4A). Under control conditions, hindlimb stimulation induced the fastest responses in L4 of the HLCx (Fig. 4B), while forelimb stimulation induced similar slope values across all layers (Fig. 4C, black traces). After SCI, slope values significantly increased in HLCx layers 4–6 in response to forelimb stimulation in group 1, but not in group 2 animals (Fig. 4C). The fastest rising slope was observed in L6 indicating a strong recruitment of neuronal population

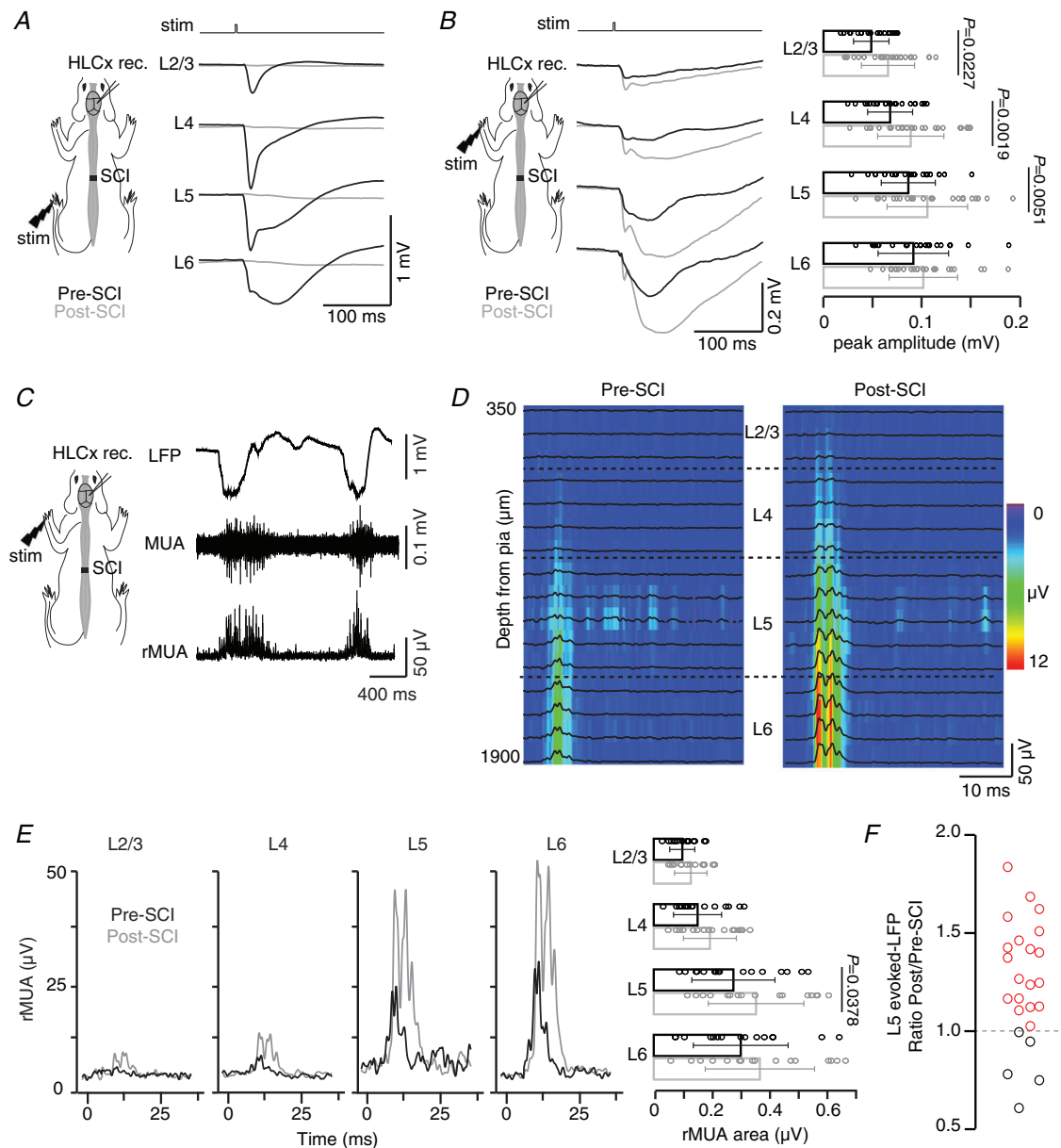


**Figure 3. Spinal cord injury induces functional changes in the HLCx in a layer-dependent manner**

**A**, schematic representation of the place of cortical recordings (HLCx rec) and hindlimb stimulation (HL stim). Examples of evoked LFP averaged across electrode sites within each layer recorded in HLCx in response to HL stim (5 mA) in control (Pre SCI, black) and after SCI (Post SCI, grey). Note that complete spinal cord transection was confirmed by absence of evoked LFP in HLCx. **B**, left, representation of HLCx rec and forelimb stimulation (FL stim) used for **B–F**. Examples of averaged evoked LFP recorded in HLCx in response to FL stim (5 mA) in control and after SCI. Bar graphs with superimposed scatter plot showing means  $\pm$  SD of the evoked LFP amplitude pre- (black) and post-SCI (grey) ( $n = 24$ ). Circles represent individual values. **C**, signal processing approach used to extract the multi-unit activity: low frequency components corresponding to local field potentials in the original traces (top) were removed with a bandpass filter (FIR bandpass filter, 0.3–3 kHz, gap 0.12 kHz) to obtain multi-unit activity (MUA, middle). Filtered MUA was then rectified and downsampled to 2 kHz for faster processing (rMUA, bottom). The area of the rectified MUA was then calculated to plot the populational response. **D**, representative laminar profile of evoked rMUA (black traces) overlapped to a colour map of the averaged HLCx responses to FL stim at 5 mA pre- and post-SCI. Dashed lines represent layer boundaries. **E**, left, averaged evoked rMUA across electrodes within distinct layers pre- and post-SCI. Right, bar graph with superimposed scatter plot showing means  $\pm$  SD of the evoked rMUA area pre- (black) and post-SCI (grey) ( $n = 19$  rats). Circles represent individual values. **F**, scatter plot showing ratio of layer 5 response magnitude calculated from evoked LFP post-/pre-SCI. Dashed line represents ratio = 1 (red circles: ratio > 1, black circles: ratio < 1). Example traces in **A–E** are representative from the same animal. See also Table 2 for a statistical summary. [Colour figure can be viewed at [wileyonlinelibrary.com](http://wileyonlinelibrary.com)]

**Table 2. Related to Fig. 3, evoked LFP and rMUA recorded in the deafferented HLCx in response to forelimb stimulation**

	Group	mA	Lesion effect	Layer effect	Lesion × Layer effect	Post hoc Tukey
LFP amplitude (mV)	All	0.5	$F_{(1,92)} = 51.8$ $P < 0.0001$	$F_{(3,92)} = 3.2$ $P = 0.0256$	$F_{(3,92)} = 0.2$ $p = 0.9198$	L2/3 $P = 0.0555$ L4 $P = 0.0059$ L5 $P = 0.0033$ L6 $P = 0.0150$
		5	$F_{(1,91)} = 50.2$ $P < 0.0001$	$F_{(3,91)} = 10.3$ $P < 0.0001$	$F_{(3,91)} = 0.3$ $P = 0.8074$	L2/3 $P = 0.0227$ L4 $P = 0.0019$ L5 $P = 0.0051$ L6 $P = 0.1130$
rMUA area ( $\mu V$ )	All	5	$F_{(1,60)} = 18.1$ $P < 0.0001$	$F_{(3,60)} = 12.5$ $P < 0.0001$	$F_{(3,60)} = 1.2$ $P = 0.3145$	L2/3 $P = 0.9945$ L4 $P = 0.6444$ L5 $P = 0.0378$ L6 $P = 0.1315$
LFP amplitude (mV)	Group 1 (79%)	0.5	$F_{(1,72)} = 48.5$ $P < 0.0001$	$F_{(3,72)} = 2.3$ $P = 0.0846$	$F_{(3,72)} = 0.2$ $P = 0.9028$	L2/3 $P = 0.0924$ L4 $P = 0.0136$ L5 $P = 0.0048$ L6 $P = 0.0151$
		5	$F_{(1,72)} = 125$ $P < 0.0001$	$F_{(3,72)} = 7$ $P = 0.0003$	$F_{(3,72)} = 0.5$ $P = 0.6790$	L2/3 $P = 0.0004$ L4 $P = 0.0001$ L5 $P = 0.0001$ L6 $P = 0.0002$
rMUA area ( $\mu V$ )	Group 1 (79%)	5	$F_{(1,47)} = 25.5$ $P < 0.0001$	$F_{(3,47)} = 9.5$ $P < 0.0001$	$F_{(3,47)} = 1$ $P = 0.4020$	L2/3 $P = 0.9101$ L4 $P = 0.3758$ L5 $P = 0.0148$ L6 $P = 0.0643$
LFP amplitude (mV)	Group 2 (21%)	0.5	$F_{(1,16)} = 4.5$ $P = 0.050$	$F_{(3,16)} = 0.8$ $P = 0.5111$	$F_{(3,16)} = 0.1$ $P = 0.9493$	
		5	$F_{(1,15)} = 15.2$ $P = 0.0014$	$F_{(3,15)} = 4.2$ $P = 0.0250$	$F_{(3,15)} = 1.8$ $P = 0.1826$	L2/3 $P = 0.9998$ L4 $P = 0.9085$ L5 $P = 0.1163$ L6 $P = 0.1218$
rMUA area ( $\mu V$ )	Group 2 (21%)	5	$F_{(1,8)} = 0.5$ $P = 0.5111$	$F_{(3,8)} = 4.1$ $P = 0.0492$	$F_{(3,8)} = 0.1$ $P = 0.9725$	

Two-way repeated measures ANOVA for comparisons between pre- and post-lesion responses across layers in response to forelimb stimulation ( $n = 24$  rats, Group = All). *Post hoc* test is described just for comparisons between conditions (lesion effect). Same analysis was performed for group 1 ( $n = 19/24$  for LFP and  $16/19$  for rMUA, 79%) and group 2 ( $n = 5/24$  for LFP and  $3/19$  for rMUA, 21%).

after SCI as can be observed by a shorter time-to-peak values (Fig. 4D).

Next, we determined the response latencies for each electrode site and for spatially averaged responses within electrodes from the same layer to create a spatiotemporal profile of the response onset (Fig. 5). Onset responses from LFP and rMUA were obtained by fitting a sigmoid function to the data and then computing the maximum curvature as described in Fedchyshyn and Wang (2007) (see Methods). Figure 5A and B shows an example of a laminar LFP profile and averaged onset latencies obtained from HLCx in response to hindlimb stimulation in control conditions. In this case, activity originated in upper middle layers and spread upwards and downwards resembling the propagation of evoked activity typically seen in distinct cortices (Schroeder *et al.* 1998; Sakata

& Harris, 2009). Next, we analysed the evoked LFP onset in response to forelimb stimulation, which could indicate how the corticocortical connectivity between HL and FL cortices is organized. The averaged onset of the animals was found to be similar across all layers with higher probability to be initiated in infragranular layers (87.5%; Fig. 5C–E pre-SCI, black traces). These data indicate that population activity measured as LFP in response to peripheral forelimb stimulation reaches HLCx almost simultaneously, as previously reported using voltage-sensitive dyes (Wester & Contreras, 2012). Such a pattern of activity onset was strongly affected by sensory deprivation in a layer-dependent manner. Infragranular layers presented a significant delay in the onset of the evoked responses, while onsets in granular and supra-granular layers were not affected (Fig. 5C–E post-SCI). In

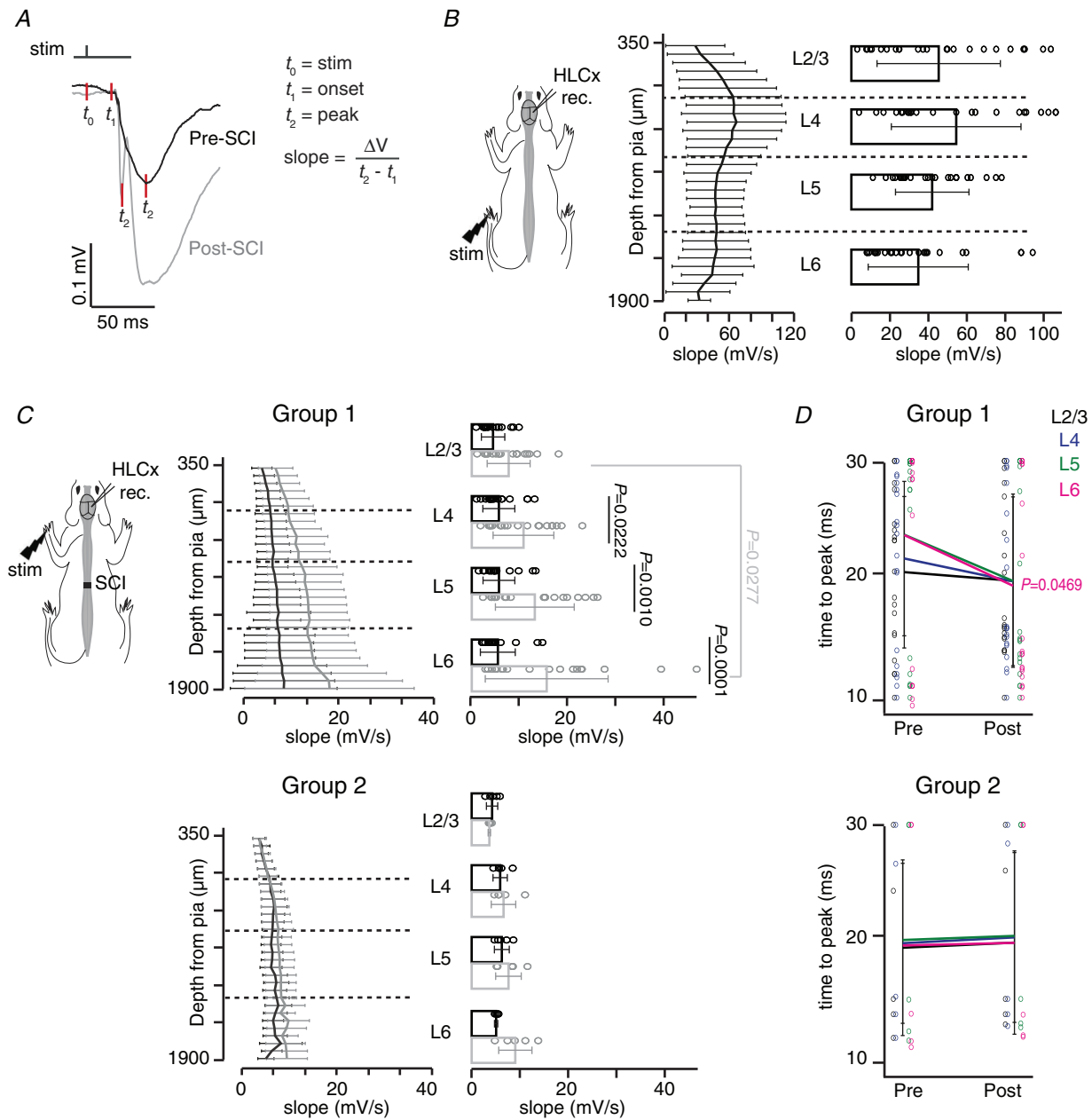


**Figure 4. Laminar profile properties of evoked responses following SCI**

*A*, original traces of averaged evoked LFP in response to FL stim pre- (black) and post-SCI (grey) illustrating the parameters used for slope analysis. *B*, schematic illustration of an animal showing the place of cortical recordings (HLCx rec) and hindlimb stimulation (HL stim). Averaged slope of evoked LFP from HLCx in response to HL stim at 5 mA in control conditions. Bar graph and scatter plot show the averaged slope values across electrodes within the same layer ( $n = 24$  rats, one-way ANOVA<sub>layer</sub>  $F_{(3,90)} = 1.9$ ,  $P = 0.1265$ ). *C*, right, evoked LFP slope obtained from HLCx in response to FL stim at 5 mA pre- and post-SCI for animals within group 1 (top,  $n = 19$ ) and group 2 (bottom,  $n = 5$ ). Left, bar graph and scatter plot showing the averaged slope of evoked LFP from HLCx in response to FL stim at 5 mA pre- and post-SCI for animals within group 1 (top, repeated measures ANOVA<sub>SCI×layer</sub>  $F_{(3,70)} = 2.1$ ,  $P = 0.1031$ , SCI effect  $F_{(1,70)} = 60.1$ ,  $P < 0.0001$ ) and group 2 (bottom, repeated measures ANOVA<sub>SCI×layer</sub>  $F_{(3,14)} = 1.3$ ,  $P = 0.3082$ , SCI effect  $F_{(1,14)} = 4.9$ ,  $P = 0.0448$ ). *D*, time-to-peak ( $t_2 - t_0$ ) of the evoked LFP responses pre- and post-SCI for group 1 (top, repeated measures ANOVA<sub>SCI×layer</sub>  $F_{(3,72)} = 1.5$ ,  $P = 0.2122$ , SCI effect  $F_{(1,72)} = 15.9$ ,  $P = 0.0002$ ) and group 2 (bottom, repeated measures ANOVA<sub>SCI×layer</sub>  $F_{(3,16)} = 0.1$ ,  $P = 0.9505$ , SCI effect  $F_{(1,16)} = 5.2$ ,  $P = 0.0368$ ). Graphs show means  $\pm$  SD. Circles represent individual values. [Colour figure can be viewed at [wileyonlinelibrary.com](http://wileyonlinelibrary.com)]

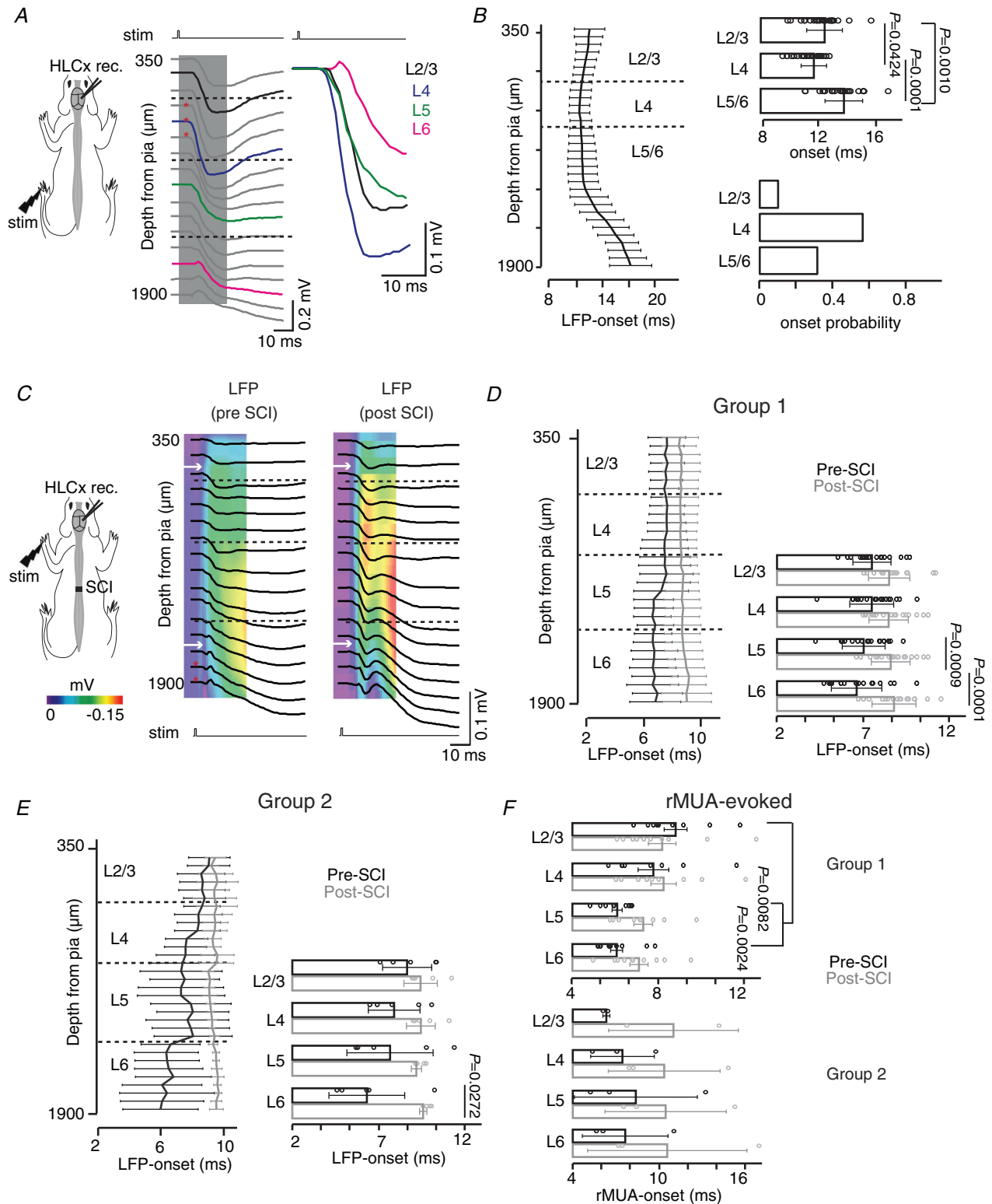


**Figure 5. Deprived infragranular layers exhibit delayed evoked-onset responses**

A, left, onset profile of evoked LFP in HLCx in response to HL stim pre-SCI. Red indicates electrodes in which evoked response started. Grey area indicates the period of response onset taken to highlighted LFP traces (in black) on the right. B, left, latency-onset averaged profile to HL stim (5 mA). Note the onset in the thalamorecipient granular layer 4. Right top, bar graph of the evoked LFP onset ( $n = 24$ , one-way ANOVA<sub>layer</sub>  $F_{(2,68)} = 19.8$ ,  $P < 0.0001$ ). Right bottom, normalized bar graph of the evoked LFP onset probability from the same population. C, onset profiles from

the same animal pre- and post-SCI showing averaged evoked LFP in HLCx in response to FL stim represented as in A, overlapped on colour maps of the LFP amplitudes from the same traces. White arrows indicate the onset response in L2/3 and L6. D and E, latency-onset of the evoked LFP represented as a laminar profile (left) or averaged across layers (right) to FL stim (5 mA) for group 1 (D,  $n = 19$ , repeated measures ANOVA<sub>SCI×layer</sub>  $F_{(3,72)} = 2.5$ ,  $P = 0.0645$ , SCI effect  $F_{(1,72)} = 65.1$ ,  $P < 0.0001$ ) and group 2 (E,  $n = 5$ , repeated measures ANOVA<sub>SCI×layer</sub>  $F_{(3,14)} = 1.7$ ,  $P = 0.2049$ , SCI effect  $F_{(1,14)} = 29.0$ ,  $P = 0.0001$ ). F, latency-onset quantified from evoked rMUA in group 1 (left,  $n = 13$ , repeated measures ANOVA<sub>SCI×layer</sub>  $F_{(3,32)} = 2.7$ ,  $P = 0.0629$ , SCI effect  $F_{(1,32)} = 7.9$ ,  $P = 0.0084$ ) and group 2 (right,  $n = 3$ , repeated measures ANOVA<sub>SCI×layer</sub>  $F_{(3,6)} = 0.4$ ,  $P = 0.7550$ , SCI effect  $F_{(1,6)} = 1.6$ ,  $P = 0.2560$ ). Graphs show means  $\pm$  SD. Circles represent individual experiments. [Colour figure can be viewed at [wileyonlinelibrary.com](http://wileyonlinelibrary.com)]

addition, onset probability was also similar across layers after SCI. In this case, both groups of animals showed similar functional changes for onset-latency responses (Fig. 5D group 1, Fig. 5E group 2). We then analysed the onset pattern of the evoked rMUA (Fig. 5F). Before SCI, HLCx infragranular layers of group 1 exhibited faster onset latencies than supragranular layers with neuronal firing originating mostly in infragranular layer 6. After SCI, differences in onset responses disappeared due to rMUA of infragranular layers tending to be delayed (Fig. 5F, left graph). Group 2 showed high variability due to the small sample ( $n = 3$ ; Fig. 5F, right graph).

### SCI induces delayed thalamocortical inputs to the deprived cortex

A possible mechanism leading to the delayed LFP and rMUA onsets in infragranular layers would be that SCI induces changes in the two main neuro-

nal pathways that drive the peripheral information from forelimbs to HLCx: (1) a canonical corticocortical pathway in which synaptic inputs from the thalamic forelimb region routes to FLCx and then reaches HLCx mostly through L2/3: FL–Th→FLCx→HLCx; and (2) a non-canonical thalamocortical pathway involving the activation of a subset of HL neuronal population in the thalamus that project to HLCx in response to forelimb stimulation: FL–Th→HLCx (Fig. 6A; Francis *et al.* 2008; Alonso-Calviño *et al.* 2016). Considering that delayed onset was observed in both HL and FL thalamus immediately after SCI (Alonso-Calviño *et al.* 2016), we wanted to determine which thalamocortical pathway was the most plausible to be involved in the delayed HLCx evoked responses. For this, we analysed simultaneous electrophysiological recordings from FLCx and HLCx obtained from tungsten electrodes located on layer 5 of both cortical regions under control conditions and after SCI (Fig. 6B; data obtained simultaneously with thalamic data published in Alonso-Calviño *et al.*

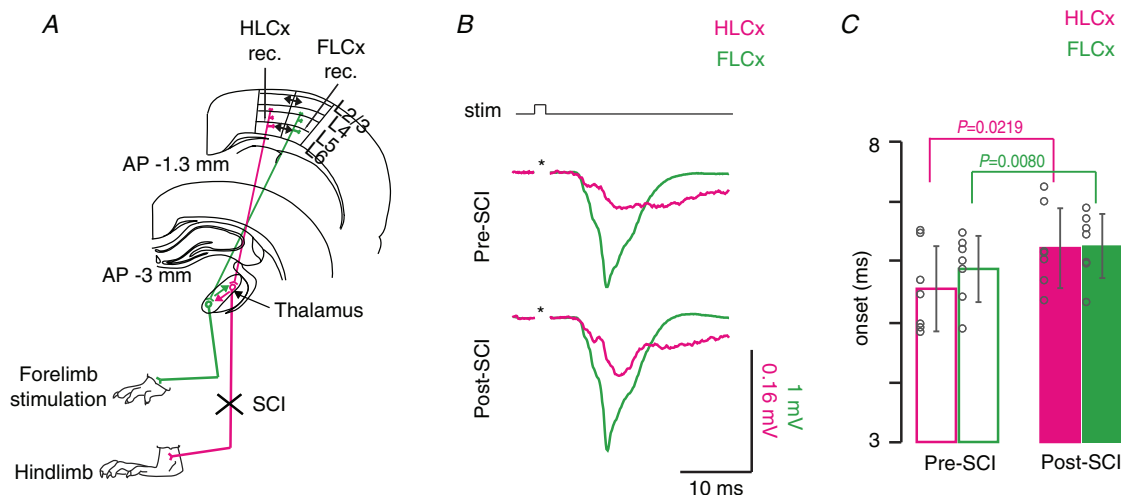


**Figure 6. Thalamocortical responses in HL cortex are delayed after SCI**

A, schematic representation of the thalamocortical pathways activated after forelimb and hindlimb stimulation. Extracellular recordings were simultaneously obtained from L5 of HLCx and FLCx while forelimb stimulation at 5 mA was applied. Coloured arrows in thalamic nucleus represent the collaterals allowing reciprocal activation of neighbouring regions. B, original field potential traces obtained from simultaneous recordings from HLCx (magenta traces) and FLCx (green traces) before and after SCI in response to FL stim. C, bar graph displaying averaged onset latencies from evoked responses in HLCx (magenta) and FLCx (green) pre- and post-SCI (open and filled bars, respectively). Data are means  $\pm$  SD. Circles represent individual values.  $n = 7$  rats, paired  $t$ -test with Bonferroni correction for two comparisons. [Colour figure can be viewed at [wileyonlinelibrary.com](http://wileyonlinelibrary.com)]

(2016)). We postulated that if increased response latencies of HLCx after SCI were induced by changes in the canonical pathway, then synaptic inputs would arrive earlier at the FLCx than at the HLCx. On the other hand, if the non-canonical pathway produces the longer latency of HLCx evoked responses, then both cortical regions should exhibit similar latencies after forelimb stimulation. Our results demonstrated that both the intact FLCx and the sensory deprived HLCx showed similar increased latencies to peripheral FL stimulation immediately after SCI with no differences between them (Fig. 6C, pre-SCI  $P = 0.2190$  and post-SCI  $P = 0.8889$ ). Therefore, increased latency of cortical evoked responses could be at least in part due to longer latencies that take place in thalamic VPL corresponding to HL and FL as described in Alonso-Calviño *et al.* (2016). Moreover, we cannot discard other intrinsic properties or corticocortical mechanisms involved in this process.

### Spontaneous activity is determined by cortical layer properties under control conditions and after sensory deprivation

Cortical spontaneous activity in anaesthetized animals is generally dominated by slow-wave activity (SWA; Fig. 7A). SWA is mainly originated from local neuronal networks and corticocortical connections (Sanchez-Vives & McCormick, 2000; Chauvette *et al.* 2010) and is importantly modulated by sensory inputs reaching the cortex throughout the thalamic pathways (Rigas & Castro-Alamancos, 2009). In this context, we have previously demonstrated that the drastic sensory loss after SCI reduces the neuronal excitability during cortical SWA (Aguilar *et al.* 2010; Fernández-López *et al.* 2019). As these data were obtained from deprived HLCx layer 5 neurons and SWA up-states propagate vertically across layers *in vitro* and *in vivo* (Sanchez-Vives & McCormick, 2000; Sakata and Harris, 2009), we calculated the onset of the spontaneous activity to determine the pattern of vertical propagation in our experimental conditions from group 1 animals. Before SCI, spontaneous up-states were initiated in any cortical layers (Fig. 7B), with infragranular layers 5 and 6 showing the highest onset probability (~70%), which corroborates previous findings in somatosensory cortex of anaesthetized rats (Sakata & Harris, 2009; Fiáth *et al.* 2016). After SCI, we found that although spontaneous up-states also tend to start in infragranular layers, this probability decreased to ~50%. This effect was achieved by a parallel increase in the probability of up-states starting at L2/3 (Fig. 7B). By analysing the rate of neuronal activity transfer across layers, we observed that up-states that originated in L2/3 (Figs 7C and D) propagated downwards with similar velocities before and after, whereas spontaneous activity that originated in deep

layers propagated upwards at a velocity much slower after SCI than in control conditions (Figs 7E and F). These data indicate that SCI induced immediate changes in the neuronal network of the deprived cortical column that slowed down the propagation of spontaneous activity that originated in infragranular layers. In addition, the increased probability of spontaneous up-state initiation in L2/3 indicates a plausible enhancement of corticocortical connections between HL and FL that helps to propagate spontaneous activity from the adjacent FLCx.

Changes in the generation of spontaneous activity may indicate that other cortical features could be affected by SCI. Following this idea, we considered that alterations of intrinsic excitability should also be reflected in the frequencies of the LFP signal in each layer during spontaneous activity from group 1 animals (Fig. 8). Spectrogram analysis performed on individual traces from L2/3, L4 and L5/6 layers (example red traces on Fig. 8A) confirmed the presence of slow (0.1–9 Hz) and fast (10–80 Hz) rhythms during up-states before SCI (Fig. 8B). Interestingly, our spectrogram analysis showed an increased relative power of fast rhythms mainly in supragranular layers following immediate SCI. Changes in the internal frequencies within up-states after SCI can be clearly observed by the fast oscillations (band-pass filtered 25–80 Hz) shown in the original traces in Fig. 9C (lower traces). To explore such frequency differences in a systematic manner, we performed a power spectrum analysis (using a fast Fourier transform, see Methods) of the LFP frequency content that was divided into different bands: SWA (0.1–1 Hz), delta (1–4 Hz), theta (4–8 Hz), alpha (8–12 Hz), beta (12–25 Hz), low gamma (25–50 Hz) and high gamma (50–80 Hz). Our data showed that from all the studied frequency bands, the relative power of the high gamma was consistently increased in supragranular layers following a SCI (Fig. 8D) while SWA, which characterized the cortical state imposed by the anaesthesia, did not change. The rest of the studied frequency bands were not altered by SCI, as statistically summarized in Table 3. Therefore, a massive sensory loss produced by an immediate SCI has different effects on the intrinsic excitability of cortical layers characterized by lower ability of layer 5 to generate up-states and increased gamma frequency in supragranular layers during spontaneous activity.

## Discussion

Here we investigated the immediate effects that a robust sensory deprivation induces in distinct layers of the primary somatosensory cortex. Our study provides strong evidence that acute SCI induces layer-dependent changes in local circuits mediating evoked and spontaneous activity in the deprived cortical region through alterations

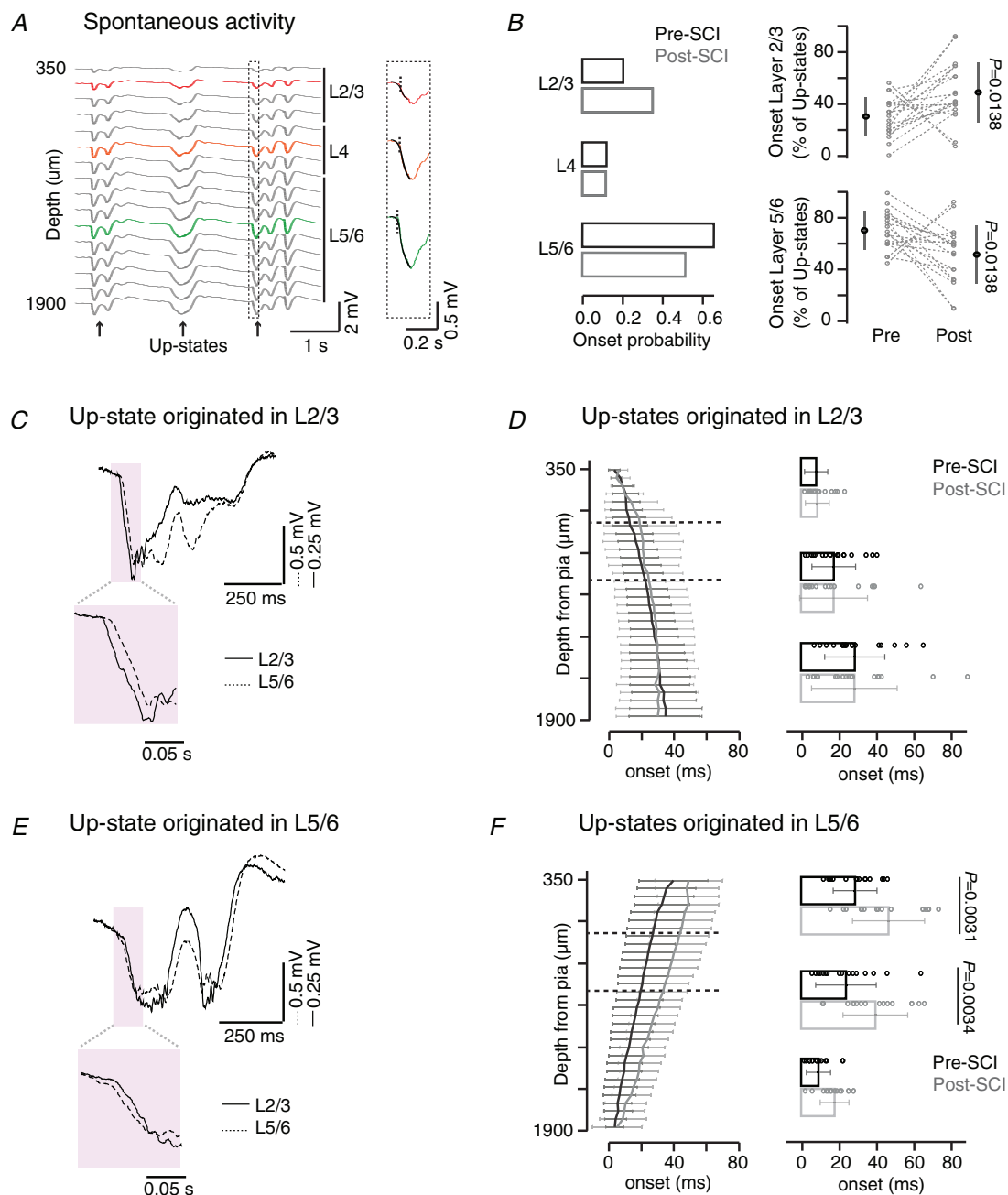


**Figure 7. Onset and propagation of spontaneous up-states is altered after SCI**

A, SWA across electrodes (left) showing insets of the sigmoid fitting used to calculate the onset latency (right). Colours indicate distinct layers. B, left, histogram of onset probability across layers of spontaneous up-states pre- and post-SCI. Right, percentage of up-states with origin in L2/3 or L5/6 pre- and post-SCI. Lines represent each individual onset probability. Black circles are means  $\pm$  SD ( $n = 24$  rats, paired  $t$ -test). C, representative example of spontaneous up-state with origin in L2/3 (black line) and delayed L5/6 (dotted line). D, laminar profile and layer-averaged onset latencies of up-states originating in layer 2/3 ( $n = 18$ ; repeated measures ANOVA<sub>SCI $\times$ layer</sub>  $F_{(2,49)} = 0.02$ ,  $P = 0.9852$ , SCI effect  $F_{(1,49)} = 0.01$ ,  $P = 0.9426$ ). E, representative example of spontaneous up-state with origin in layer 5/6 (dotted line) and delayed L2/3 (black line). F, laminar profile and averaged onset latencies of up-states originating in layer 5/6 ( $n = 16$ , repeated measures ANOVA<sub>SCI $\times$ layer</sub>  $F_{(2,43)} = 1.1$ ,  $P = 0.3313$ , SCI effect  $F_{(1,43)} = 33.9$ ,  $P < 0.0001$ ). Insets in C and E are magnification of magenta areas in the time axis. Graphs show means  $\pm$  SD. Circles represent individual values. [Colour figure can be viewed at [wileyonlinelibrary.com](http://wileyonlinelibrary.com)]

of both corticocortical and thalamocortical connections (Fig. 9). Regarding evoked responses, sensory deprivation potentiated the response magnitude and rising population neuronal activity of infragranular layers (L5/6) of the deprived HLCx. On the other hand, the study of

spontaneous activity show that supragranular layer 2/3 is the most affected by SCI exhibiting increased probability to initiate spontaneous up-states and increased power of high-frequency oscillations in the gamma band spectrum. Therefore, our results show that local

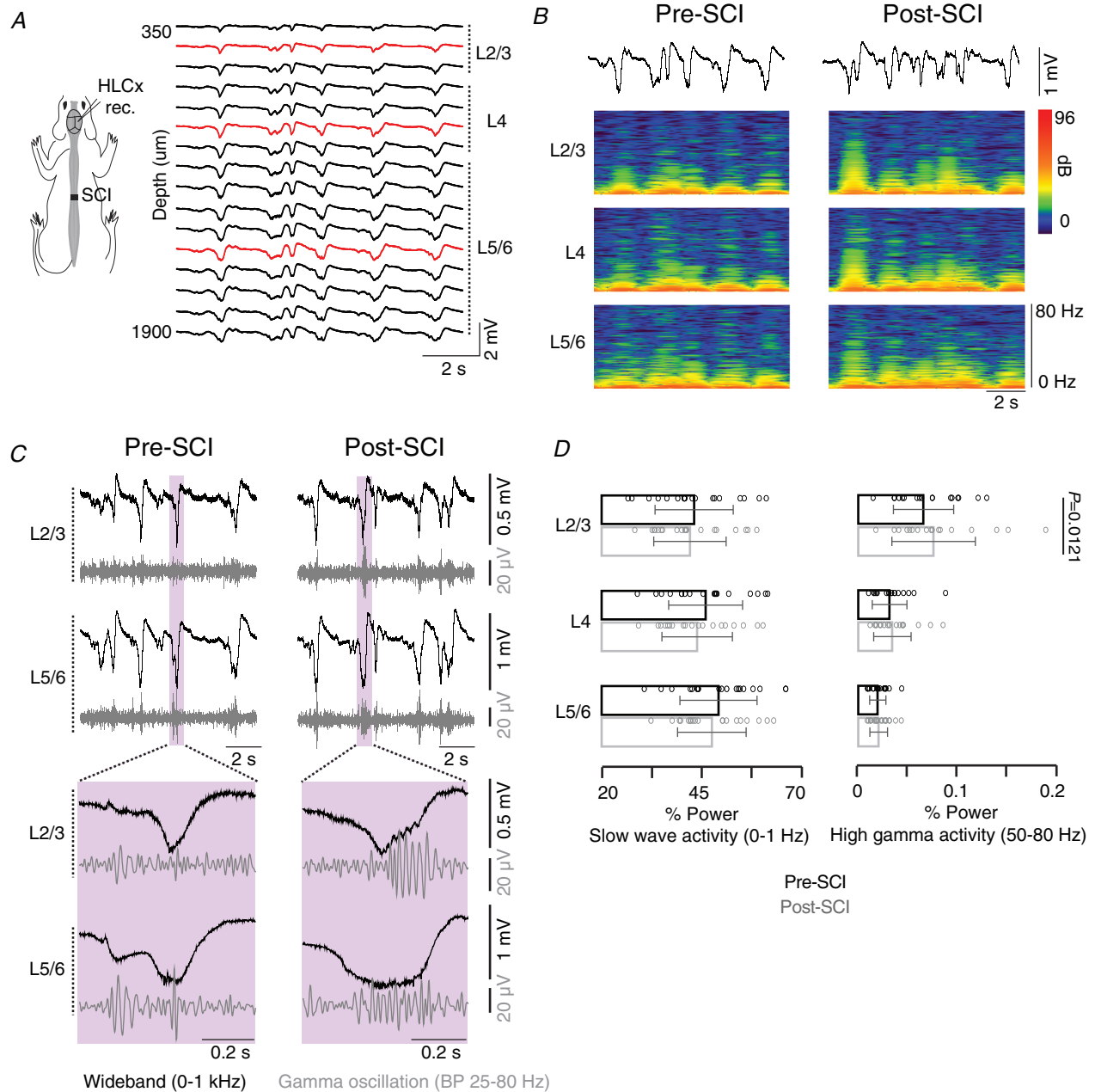


**Figure 8. SCI increases high-gamma frequency oscillations in supragranular layers**  
 A, example of spontaneous SWA profile recorded from HLCx in control conditions. Red traces represent selected electrodes within each cortical layer used for B and C. B, colour plots showing spontaneous spectrogram in L2/3, L4 and L5/6 pre- and post-SCI. C, wideband signal (black) and gamma-filtered (25–80 Hz, grey) traces of SWA from L2/3 and L5/6 with expanded traces of the indicated time window. D, SWA (repeated measures ANOVA<sub>SCI×layer</sub>  $F_{(2,54)} = 0.2, P = 0.8202$ , SCI effect  $F_{(1,54)} = 5.5, P = 0.0231$ ) and gamma (repeated measures ANOVA<sub>SCI×layer</sub>  $F_{(2,51)} = 2.9, P = 0.0630$ , SCI effect  $F_{(1,51)} = 8.0, P = 0.0066$ ) relative power from distinct layers before and after SCI from group 1 ( $n = 19$ ). Graphs show means  $\pm$  SD. Circles represent individual values. See also Table 3 for statistical summary for all frequency bands. [Colour figure can be viewed at [wileyonlinelibrary.com](http://wileyonlinelibrary.com)]

neuronal and network properties of each cortical layer are responsible for differential effects observed in the deprived somatosensory cortex after SCI.

**Layer-dependent changes in sensory-evoked responses after SCI**

Sensory deprivation has dramatic effects on the organization of brain circuitry, leading to a takeover of the deprived cortex by other cortical areas. This process is initiated as soon as deprivation occurs (Humanes-Valera *et al.* 2013) and continues in a time scale from days to months (Endo *et al.* 2007; Sydekum *et al.* 2014; Humanes-Valera *et al.* 2017; Fernández-López *et al.* 2019). In the case of SCI, the reorganization of the deprived cortex leads to the acquisition of new sensory functions that could help functional recovery (Rossignol & Frigon, 2011) as well as initiating such associated pathologies as pain and spasticity (Siddall & Loeser,

2001). The mechanisms driving beneficial or detrimental reorganization are unknown, but could rely on the complex laminar organization of cortical areas known to have distinct cellular composition and intrinsic circuitry. Therefore, a better knowledge of the contribution of each cortical layer to the well-known phenomenon of CoRe after sensory deprivation is required. In this study, we have included for the first time the perspective of a role for cortical layering in the cortical changes after SCI, which could explain initiation and complexity of CoRe as well as the variability between individuals as observed in human patients.

Previously, differences among layers were only addressed in a neonatal SCI model in which the effects of exercise in the cortical long-term plasticity were studied (Kao *et al.* 2009). Our present data go further to demonstrate that neuronal activity is differentially affected across layers of the sensory-deprived HLCx immediately after a SCI in adult individuals. Under our experimental conditions, increased magnitude of evoked LFP in

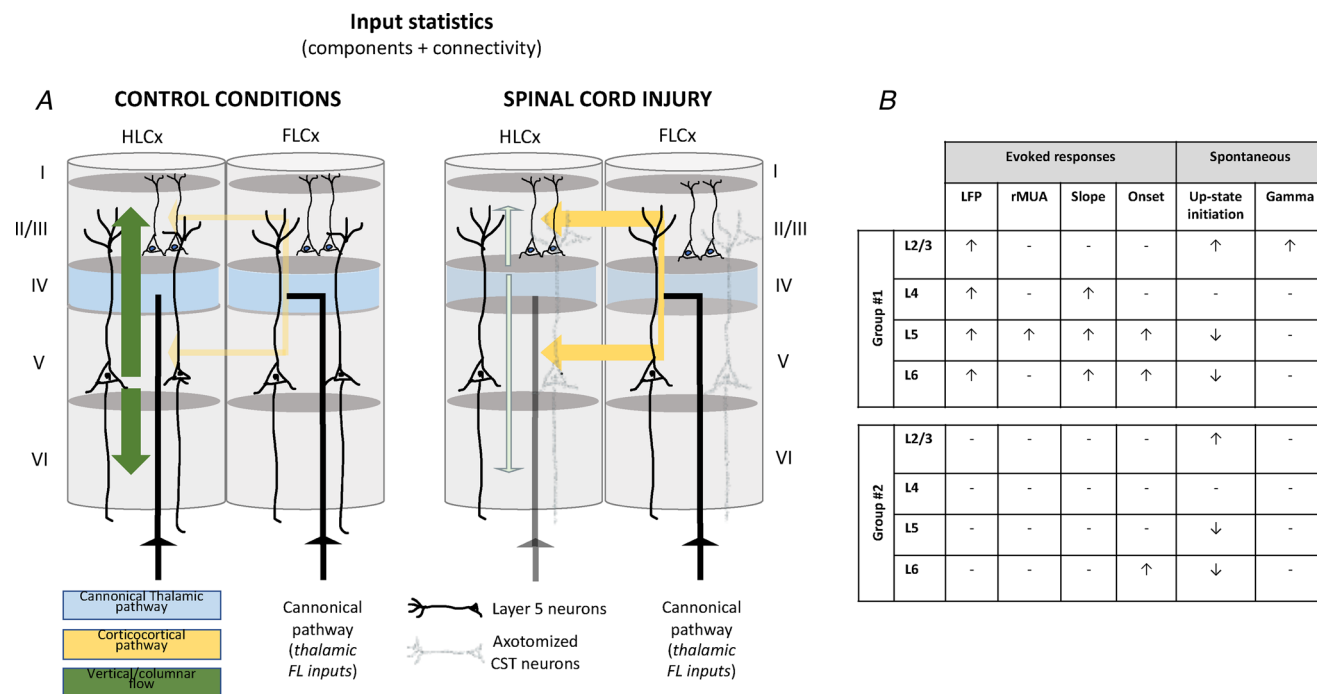


**Figure 9. Summary of the findings highlighting the altered weight of synaptic inputs within and between regions of the hindlimb and forelimb cortices**

A, in control conditions, spontaneous cortical activity is settled by a balance between components (i.e. neurons and other cell components such as glial cell types) and connectivity from thalamic and adjacent cortical regions. In this condition and upon arrival of sensory information to a non-corresponding somatosensory area, the recurrent, columnar activity at the hindlimb cortex prevails over other types of connectivity such as corticocortical ones. Immediately after SCI, the deafferentation of the hindlimb cortex produces an altered input statistic in the columnar region as a result of loss of direct thalamic inputs compounded with physiological changes in the axotomized corticospinal (CST) neurons. Such physiological effect facilitates the arrival of corticocortical inputs from adjacent, intact regions (i.e. forelimb cortex). In this sense, our data reveal that the corticocortical connectivity differs among layers, which could represent the first step to initiating the long-term cortical reorganization in a layer-dependent manner. B, summary table illustrating the overall effects of a SCI on distinct features of evoked and spontaneous cortical activity in the deafferented cortex. [Colour figure can be viewed at [wileyonlinelibrary.com](http://wileyonlinelibrary.com)]

**Table 3.** Related to Fig. 8, frequency content across layers of HLCx before and immediately after a SCI

	Lesion effect	Layer effect	Lesion*Layer effect	Post hoc Tukey
SWA	$F_{(1,54)} = 5.5$ $P = 0.0231$	$F_{(2,54)} = 2.1$ $P = 0.1360$	$F_{(2,54)} = 0.2$ $P = 0.8202$	L2/3 $P = 0.9491$ L4 $P = 0.4926$ L5/6 $P = 0.7288$
$\delta$	$F_{(1,54)} = 3.5$ $P = 0.0669$	$F_{(2,54)} = 0.9$ $P = 0.4120$	$F_{(2,54)} = 0.3$ $P = 0.7614$	
$\theta$	$F_{(1,54)} = 8.9$ $P = 0.0044$	$F_{(2,54)} = 10.4$ $P = 0.0002$	$F_{(2,54)} = 0.1$ $P = 0.9038$	L2/3 $P = 0.3523$ L4 $P = 0.4925$ L5/6 $P = 0.7407$
$\alpha$	$F_{(1,51)} = 8.9$ $P = 0.0199$	$F_{(2,51)} = 31.1$ $P < 0.0001$	$F_{(2,51)} = 0.3$ $P = 0.7472$	L2/3 $P = 0.5299$ L4 $P = 0.9674$ L5/6 $P = 0.5805$
$\beta$	$F_{(1,51)} = 2.7$ $P = 0.1044$	$F_{(2,51)} = 28$ $P < 0.0001$	$F_{(2,51)} = 0.1$ $P = 0.8946$	
Low $\gamma$	$F_{(1,51)} = 4.9$ $P = 0.0308$	$F_{(2,51)} = 15.8$ $P < 0.0001$	$F_{(2,51)} = 1.3$ $P = 0.2722$	L2/3 $P = 0.1119$ L4 $P = 0.9910$ L5/6 $P = 0.9878$
High $\gamma$	$F_{(1,51)} = 8.0$ $P = 0.0066$	$F_{(2,51)} = 23.5$ $P < 0.0001$	$F_{(2,51)} = 2.9$ $P = 0.0630$	L2/3 $P = 0.0121$ L4 $P = 0.9254$ L5 $P = 0.9993$

Two-way ANOVA of the relative power spectrum of each band frequency in the spontaneous activity fast Fourier transform analysis. *Post hoc* significance is described just for comparisons between conditions in the same layer (lesion effect). Analysis from group 1 animals ( $n = 19$  rats).

response to stimulation of the contralateral forelimb was observed across layers of the deprived cortex (Fig. 2B), which is highly consistent with results obtained using brain scanning approaches (Endo *et al.* 2007; Ghosh *et al.* 2010). This effect could be explained by the anatomical and functional overlapping of hindlimb and forelimb cortical areas (Moxon *et al.* 2008; Morales-Botello *et al.* 2012), in which corticocortical excitatory inputs may become unmasked following SCI and increase the responses to stimulation of a non-corresponding extremity (i.e. forelimb). In addition, we have previously shown that SCI increases neuronal responses in the thalamic hindlimb region to forelimb stimulation (Alonso-Calviño *et al.* 2016). Therefore, changes in thalamic excitability could also play a direct role in the increased cortical responses of sensory deprived HLCx. The initial slopes of evoked LFP, often used to determine changes in the arrival and/or synchronization of synaptic inputs and usually affected by changes in the excitation–inhibition balance, were significantly faster in granular and infragranular neurons (Fig. 4C). Since cortical layers are known to display different inhibitory features (Wilent & Contreras, 2004), our data showing changes in the LFP slope in a layer-dependent manner suggest that local network properties are differentially affected by SCI and could represent an unequal reduction of local inhibition across layers allowing infragranular cells to better integrate evoked sensory inputs.

Our data also identified a subset of animals (21%) that consistently did not show immediate neuronal changes related to either evoked responses or spontaneous activity. It is thought that the degree of cortical reorganization can be attributed to several variables including species, age, behavioural activity and therapy regimes after the injury (Moxon *et al.* 2014; Jutzeler *et al.* 2018). Since we did not find any differences regarding age, sex or anatomical location of the electrode, we postulate that the population that did not exhibit changes in the cortical activity may result from our acute model of SCI (i.e. from minutes to a few hours), which does not exclude the possibility that these animals present cortical changes in sub-acute and/or chronic phases of the injury. The presence of some spared fibres close to the lateral and/or ventral bone that were not fully transected after our spinal cord injury could also be a source of variability leading to the group separation. However, considering the physical and physiological assessment performed after SCI to determine the total disconnection from spinal cord to brain, we see this possibility as unlikely.

Electrophysiological recordings of LFP and action potentials reflect different but complementary aspects of neuronal processing. While LFP integrates subthreshold activity as synaptic inputs and membrane potentials from a neuronal population in a given region, action potentials are the output signals from individual neurons close to the recording electrode. Contrary to the homogeneous

increase in the evoked LFP after SCI through L2/3–L5, we found striking differences among layers regarding MUA. In this case, sensory deprivation increased neuronal excitability in infragranular neurons of the deprived HLCx but not in granular and supragranular layers. Infragranular neurons have several characteristics that may lead to most of the changes: they receive excitatory inputs from all other cortical layers and neighbouring cortical areas (Schubert *et al.* 2007), they receive extensive thalamic inputs, and they have larger receptive fields (Tutunculer *et al.* 2006; Moxon *et al.* 2008; Rigas & Castro-Alamancos, 2009; Wester & Contreras, 2013). Therefore, changes in the local network connectivity and/or intrinsic properties of infragranular neurons are more prone to be noticed after SCI compared to other layers. Moreover, the only intracellular data obtained from infragranular neurons after acute SCI (Humanes-Valera *et al.* 2017) perfectly support the relation between the increased MUA responses and the faster slope of evoked LFP that we show in the present work. Regarding the changes in layer 5 neurons, we would like to remark that although previous data have shown preservation of L5 pyramidal neurons after axotomy due to SCI (Ghosh *et al.* 2012), we cannot discard that direct damage at the level of the spinal cord of corticospinal neurons with their origin in cortical layer 5 may have influenced some of the observed functional changes. In fact, a synaptic reorganization in terms of a retrograde dendritic spine loss of both axotomized and non-axotomized layer 5 neurons in the hindlimb somatosensory cortex has been observed a few days following SCI (Ghosh *et al.* 2012). Interestingly, the reduction in spines depends on the layer through which the same apical dendrite is passing, that is, proximal segments in layer 5a are much more vulnerable to spine loss than distal segments in layer 2/3 indicating that corticocortical connections in supragranular layers may maintain sufficient cortical activity that favours synaptic maintenance. Under our experimental conditions, it is unlikely that such drastic spine remodelling could be triggering the observed functional changes in the first few minutes after the injury, indicating the possibility of a mechanism not directly related to anatomical aspects such as changes in connectivity. However, a recent study using an *in vitro* model to study axon injury of pyramidal neurons (Nagendran *et al.* 2017) has greatly improved knowledge of the rapid effects (24–48 h) of axotomy in synaptic remodelling. It has been described that axotomized neurons undergo retrograde dendritic spine loss followed by hyper-presynaptic excitability, via elimination of inhibitory inputs onto the affected neurons. The increased neuronal excitability supports our results regarding the increased LFP and MUA responses observed in infragranular layers, especially layer 5, after a SCI. In addition, the immediate alteration in the neuronal excitability observed by our study and that could lead

to the anatomical elimination of inhibitory inputs, may set the physiological basis for the short- and long-term changes in spine density observed in Ghosh *et al.* (2012). Therefore, our data strongly indicate that excitability of infragranular neuronal networks is mostly affected in the context of evoked responses, which could be directly implicated in the mechanisms regulating subcortical output generating adaptive behaviour and functional recovery following spinal cord injury.

### SCI alters the spread of sensory-evoked activity across layers

The onset of evoked sensory responses in cortical regions is driven by synaptic inputs from corticocortical and thalamocortical connections. Our data showing almost simultaneous initiation of evoked responses between layers (Figs 5C and D) corroborate *in vitro* data showing that horizontal corticocortical connectivity with adjacent cortical areas induces similar onsets of evoked responses (Wester & Contreras, 2012). However, this feature was strongly delayed in L5/6 of the deprived cortex after SCI, which could indicate modifications in the corticocortical synaptic connectivity but also in thalamic connections that project to HLCx. *In vivo* peripheral forelimb stimulation induces strong neuronal responses in the FL area of the thalamic VPL, but also in a population of the HL area of the VPL through collaterals that finally project onto HLCx (Fig. 6A; Alonso-Calviño *et al.* 2016). By simultaneously recording neuronal activity in HLCx and intact FLCx, we showed that SCI leads to a delayed latency in the neuronal activity of both regions in response to peripheral stimulation. In addition, we did not observe changes in the onset of thalamus-devoid supragranular neurons after SCI (Fig. 6B), suggesting that the onset of evoked LFP responses in infragranular layers is more conditioned by changes in thalamic inputs. Therefore, our data indicate that although a delay in the arrival of synaptic inputs in infragranular layers is observed after SCI, these are more efficiently integrated as shown by increased slope and magnitude of evoked LFP. Then, sensory deprivation produces changes in the integration properties of local networks of the deprived infragranular neurons that could be the basis for the long-term reorganization of sensory cortex observed after SCI.

Changes in the neuronal ability to integrate synaptic inputs may lead to an altered cortical information flow transfer as previously shown by altering the development of the thalamorecipient layer 4 (McLaughlin *et al.* 2005). Under physiological conditions, cortical layers are considered functionally connected local circuits exhibiting synchronized fluctuations of neuronal activity that are transferred within (vertical flow) and between (horizontal flow) cortical columns. The strength and

the ability to integrate and transmit the information are jointly determined by the confluence of neuronal inputs from distinct brain areas (i.e. brainstem, thalamus and cortical regions), but also by the intrinsic properties of the neurons in the network hub. SCI abruptly interrupts the input statistics in the affected cortex leading to a severe disruption of information-flow highways as observed by the altered transfer of both spontaneous and evoked cortical activity (Figs. 5 and 7). In this scenario there are different possibilities. On one hand, the altered transfer of information could result from a simple change in the weight of horizontal over vertical input statistics in the affected cortex, that is, a synaptic reduction and a disruption in the coherence between layers (vertical flow) that would favour horizontal input statistics. On the other hand, a more extreme condition would be that SCI leads to a disassembling of the layering connectivity triggering neurons to work as individual nodes without statistical relationship between edges, that is, local neural circuits that are no longer functionally connected and start working as isolated, independent and non-regulated cortical hubs. In any case, SCI represents a deviation from the physiological network that could be accurately inferred and modelled in the future to study functional connectivity alterations and to determine if changes in the information flow affect the global functional network and dictate the strength of the cortical reorganization in the long-term.

### Sensory deprivation affects the generation of gamma oscillations and the propagation of up-states in the cortical column

In our experimental model, the cortical activity before SCI was settled in the state of slow-wave oscillation ( $\sim 1$  Hz) characterized by alternating periods of synchronized activation of the neuronal population (up-states) and silent periods (down-states; Sanchez-Vives & McCormick, 2000). Slow waves are the predominant cortical rhythm during rapid eye movement sleep and anaesthesia and have been linked to a variety of brain functions including homeostatic synaptic plasticity, memory consolidation, and synchronization of local and global networks. Their role in synaptic plasticity has been widely studied and it is evidenced in cortical neurons by an increased  $\text{Ca}^{2+}$  influx with subsequent activation of signalling cascades associated with increased synaptic plasticity, such as those involving  $\text{Ca}^{2+}$ /calmodulin-dependent kinase II (Yuste & Tank, 1996; Soderling & Derkach, 2000). On the other hand, the patterns of slow wave activity allow the synchronization and propagation of activity among distinct layers of a cortical column (Sanchez-Vives & McCormick, 2000) as well as the propagation to adjacent cortical regions (Welle & Contreras, 2016). Together,

synaptic plasticity and cortical activity propagation form the core of the mechanism triggering long-term cortical reorganization, raising the importance of studying detailed features of SWA following injuries. In this regard, our data using urethane as anaesthesia to artificially induce a cortical activity similar to what has been described during sleep (Clement *et al.* 2008) reveal important alterations of SWA, and therefore net synaptic strength, following SCI that could be directly related to the initiation of the cortical reorganization process.

Within slow wave oscillations, up-state events are dominated by gamma frequency activity (25–80 Hz) with implications for multiple aspects of information processing such as sensory representation (Castro-Alamancos, 2009), sensorimotor integration (Schoffelen *et al.* 2011) and cognition (Gruber *et al.* 2004). Here, we describe that deafferentation due to SCI induces a layer-specific modulation of high frequency oscillations during up-states, with the gamma range showing strikingly increased power in supragranular layers, but not in infragranular or granular layers. Layer 2/3 is known to present a network of inhibitory neurons that initiates gamma oscillations through either parvalbumin neurons (Cardin *et al.* 2009; Welle & Contreras, 2016) or somatostatin neurons (Veit *et al.* 2017). In this context, the sensory deprivation produces a reduction in the constant thalamic excitatory inputs onto the deafferented cortex that may lead to an increase of the general inhibitory tone in supragranular layers which facilitates local mechanisms of gamma oscillations. In addition to the well-described role of high frequencies in information processing, gamma oscillations have also been implicated in the formation of cortical maps during development (Minlebaev *et al.* 2011) and related to generation of pain perception in somatosensory cortex (Tan *et al.* 2019). Therefore, it is plausible that the increased gamma may comprise one of the mechanisms involved in the initiation of cortical reorganization following SCI.

Spontaneous up-states within slow-wave oscillations usually initiate in deep infragranular layers (Sakata & Harris, 2009) and depend primarily on both intrinsic properties of the cortical column and corticocortical connections (Sanchez-Vives & McCormick, 2000). Our data show that SCI increases the probability of up-state generation in layer 2/3 with a consequent decrease in layer 5/6. There are several possible mechanisms that in isolation and/or synergistically could be leading to such changes. First, subthreshold oscillations in the membrane potential during gamma oscillations facilitate the generation of spontaneous up-states (Puig *et al.* 2008). Since we also observed increased gamma in L2/3 after SCI probably due to increased activity of inhibitory neurons, this mechanism could be a trigger for the increased up-state onset (Compte *et al.* 2003). Second, we have

previously shown that SCI decreases neuronal activity during up-states in layer 5 neurons (Fernandez-Lopez *et al.* 2019), which may favour the initiation of up-states in layer 2/3 by releasing supragranular neurons from L5 to L2/3 modulation (Wester & Contreras, 2012). In the same way, *in vitro* experiments show that up-state generation in the somatosensory cortex is reduced after blocking thalamocortical inputs, while a reduction of the fast excitatory activity (mediated by AMPA receptors) increases the probability of generating up-states in cortical layer 2/3 (Favero & Castro-Alamancos, 2013). Finally, the superficial cortical layer 2/3 is also known to receive long-range axons from other cortical areas that facilitate long-range synchronization (Yamashita *et al.* 2018). We have previously shown that SCI induces neuronal changes not only in the deprived HL cortex, but also in the adjacent, intact forelimb cortex (Humanes-Valera *et al.* 2013, 2017; Yagüe *et al.* 2014). Therefore, changes in oscillatory synchronization in the sensory forelimb cortex may be transferred to the hindlimb cortex through L2/3 corticocortical connections during spontaneous activity facilitating the up-state generation within the deprived cortical column. Despite the mechanism used by the deprived cortex to generate spontaneous activity and to propagate the neuronal information across layers, the increase in L2/3 up-states may allow the deprived column to maintain its internal activity with possible implications in the processing of evoked sensory inputs as well as the reorganization of cortical areas after sensory deprivation.

Based on previous reports, there are two main factors that have been directly related to the development of CoRe: (1) structural changes of neuronal networks and connections linked to anatomical rewiring of axons and dendrites (Ghosh *et al.* 2012; Nagendran *et al.* 2017; Zhang *et al.* 2015), and (2) functional changes linked to activity-dependent plasticity and/or homeostatic plasticity (Jain *et al.* 1998, 2008; Fernández-López *et al.* 2019). Since our results were obtained in a narrow time window (from minutes to a few hours after deprivation), the possibility of structural and/or anatomical changes is limited as previously shown (Jain *et al.* 1995; Chand and Jain, 2005). On the contrary, we consider that the observed neuronal network alterations in a specific layer will depend on the importance of lacking the preferred connectivity (thalamocortical or corticocortical), the inhibitory neuronal composition, and how the network integrates non-preferential and weak connections (Endo *et al.* 2007; Ganzer *et al.* 2013; Humanes-Valera *et al.* 2017; Manohar 2017). Then, immediate functional changes described in our results point to an initiation of homeostatic processes intended to compensate input deprivation by rebalancing excitation–inhibition as has been described in other sensory systems (Keck *et al.* 2013; Teichert *et al.* 2017), which can be followed in the

long-term by a process of activity-dependent plasticity. Importantly, our work provides a new framework for a better understanding of CoRe after SCI by identifying a role for deprived supragranular layers in better integrating spontaneous corticocortical information to modify the excitability of the column, and for deprived infragranular layers in better integrating evoked sensory inputs to preserve specific corticothalamic and cortico-subcortical networks. We postulate that the layer-specific neuronal changes observed immediately after sensory deprivation may guide the long-term alterations in neuronal excitability and plasticity linked to the rearrangements of somatosensory networks and the appearance of central sensory pathologies usually associated with SCI.

## References

- Aguilar J, Humanes-Valera D, Alonso-Calviño E, Yague JG, Moxon KA, Oliviero A & Foffani G (2010). Spinal cord injury immediately changes the state of the brain. *J Neurosci* **30**, 7528–7537.
- Alonso-Calviño E, Martínez-Camero I, Fernández-López E, Humanes-Valera D, Foffani G & Aguilar J (2016). Increased responses in the somatosensory thalamus immediately after spinal cord injury. *Neurobiol Dis* **87**, 39–49.
- Bola L, Zimmermann M, Mostowski P, Jednoróg K, Marchewka A, Rutkowski P & Szwed M (2017). Task-specific reorganization of the auditory cortex in deaf humans. *Proc Natl Acad Sci U S A* **114**, E600–E609.
- Canedo A & Aguilar J (2000). Spatial and cortical influences exerted on cuneothalamic and thalamocortical neurons of the cat. *Eur J Neurosci* **12**, 2515–2533.
- Cardin JA, Carlén M, Meletis K, Knoblich U, Zhang F, Deisseroth K, Tsai LH & Moore CI (2009). Driving fast-spiking cells induces gamma rhythm and controls sensory responses. *Nature* **459**, 663–667.
- Castro-Alamancos MA (2009). Cortical up and activated states: implications for sensory information processing. *Neuroscientist* **15**, 625–634.
- Chand P & Jain N (2015). Intracortical and thalamocortical connections of the hand and face representations in somatosensory area 3b of macaque monkeys and effects of chronic spinal cord injuries. *J Neurosci* **35**, 13475–13486.
- Chauvette S, Volgushev M & Timofeev I (2010). Origin of active states in local neocortical networks during slow sleep oscillation. *Cereb Cortex* **20**, 2660–2674.
- Clancy KB, Schnepel P, Rao AT, Feldman DE (2015). Structure of a single whisker representation in layer 2 of mouse somatosensory cortex. *J Neurosci* **35**, 3946–3958.
- Clement EA, Richard A, Thwaites M, Ailon J, Peters S & Dickson CT (2008). Cyclic and sleep-like spontaneous alternations of brain state under urethane anaesthesia. *PLoS One* **3**, e2004.
- Compte A, Sanchez-Vives MV, McCormick DA & Wang XJ (2003). Cellular and network mechanisms of slow oscillatory activity (<1 Hz) and wave propagations in a cortical network model. *J Neurophysiol* **89**, 2707–2725.

- Curt A, Bruhlmeier M, Leenders KL, Roelcke U & Dietz V (2002). Differential effect of spinal cord injury and functional impairment on human brain activation. *J Neurotrauma* **19**, 43–51.
- Endo T, Spenger C, Tominaga T, Brené S & Olson L (2007). Cortical sensory map rearrangement after spinal cord injury: fMRI responses linked to Nogo signalling. *Brain* **130**, 2951–2961.
- Erchova IA, Lebedev MA & Diamond ME (2002). Somatosensory cortical neuronal population activity across states of anaesthesia. *Eur J Neurosci* **15**, 744–752.
- Favero M & Castro-Alamancos MA (2013). Synaptic cooperativity regulates persistent network activity in neocortex. *J Neurosci* **33**, 3151–3163.
- Fedchyshyn MJ & Wang LY (2007). Activity-dependent changes in temporal components of neurotransmission at the juvenile mouse calyx of Held synapse. *J Physiol* **581**, 581–602.
- Fernández-López E, Alonso-Calviño E, Humanes-Valera D, Foffani G & Aguilar J (2019). Slow-wave activity homeostasis in the somatosensory cortex after spinal cord injury. *Exp Neurol* **322**, 113035.
- Fiáth R, Kerekes BP, Wittner L, Tóth K, Beregszászi P, Horváth D & Ulbert I (2016). Laminar analysis of the slow wave activity in the somatosensory cortex of anesthetized rats. *Eur J Neurosci* **44**, 1935–1951.
- Fiáth R, Márton AL, Mátyás F, Pinke D, Márton G, Tóth K & Ulbert I (2019). Slow insertion of silicon probes improves the quality of acute neuronal recordings. *Sci Rep* **9**, 111.
- Field KJ, White WJ & Lang CM (1993). Anaesthetic effects of chloral hydrate, pentobarbitone and urethane in adult male rats. *Lab Anim* **27**, 258–269.
- Francis JT, Xu S & Chapin JK (2008). Proprioceptive and cutaneous representations in the rat ventral posterolateral thalamus. *J Neurophysiol* **99**, 2291–2304.
- Friedberg MH, Lee SM & Ebner FF (1999). Modulation of receptive field properties of thalamic somatosensory neurons by the depth of anesthesia. *J Neurophysiol* **81**, 2243–2252.
- Ganzer PD, Moxon KA, Knudsen EB & Shumsky JS (2013). Serotonergic pharmacotherapy promotes cortical reorganization after spinal cord injury. *Exp Neurol* **241**, 84–94.
- Ghosh A, Haiss F, Sydekum E, Schneider R, Gullo M, Wyss MT, Mueggler T, Baltés C, Rudin M, Weber B & Schwab ME (2010). Rewiring of hindlimb corticospinal neurons after spinal cord injury. *Nat Neurosci* **13**, 97–104.
- Ghosh A, Peduzzi S, Snyder M, Schneider R, Starkey M & Schwab ME (2012). Heterogeneous spine loss in layer 5 cortical neurons after spinal cord injury. *Cereb Cortex* **22**, 1309–1317.
- Green JB, Sora E, Bialy Y, Ricamato A & Thatcher RW (1998). Cortical sensorimotor reorganization after spinal cord injury: an electroencephalographic study. *Neurology* **50**, 1115–1121.
- Griffen TC, Haley MS, Fontanini A & Maffei A (2017). Rapid plasticity of visually evoked responses in rat monocular visual cortex. *PLoS One* **12**, e0184618.
- Gruber T, Tsivilis D, Montaldi D & Müller MM (2004). Induced gamma band responses: an early marker of memory encoding and retrieval. *Neuroreport* **15**, 1837–1841.
- Humanes-Valera D, Aguilar J & Foffani G (2013). Reorganization of the intact somatosensory cortex immediately after spinal cord injury. *PLoS One* **8**, e69655.
- Humanes-Valera D, Foffani G, Alonso-Calviño E, Fernández-López E & Aguilar J (2017). Dual cortical plasticity after spinal cord injury. *Cereb Cortex* **27**, 2926–2940.
- Jacob V, Mitani A, Toyozumi T & Fox K (2017). Whisker row deprivation affects the flow of sensory information through rat barrel cortex. *J Neurophysiol* **117**, 4–17.
- Jain N, Florence SL & Kaas JH (1995). Limits on plasticity in somatosensory cortex of adult rats: hindlimb cortex is not reactivated after dorsal column section. *J Neurophysiol* **73**, 1537–1546.
- Jain N, Florence SL & Kaas JH (1998). Reorganization of somatosensory cortex after nerve and spinal cord injury. *News Physiol Sci* **13**, 143–149.
- Jain N, Qi HX, Collins CE & Kaas JH (2008). Large-scale reorganization in the somatosensory cortex and thalamus after sensory loss in macaque monkeys. *J Neurosci* **28**, 11042–11060.
- Jutzeler CR, Streijger F, Aguilar J, Shortt K, Manouchehri N, Okon E, Hupp M, Curt A, Kwon BK & Kramer JLK (2018). Sensorimotor plasticity after spinal cord injury: a longitudinal and translational study. *Ann Clin Transl Neurol* **6**, 68–82.
- Kao T, Shumsky JS, Murray M & Moxon KA (2009). Exercise induces cortical plasticity after neonatal spinal cord injury in the rat. *J Neurosci* **29**, 7549–7557.
- Keck T, Keller GB, Jacobsen RI, Eysel UT, Bonhoeffer T & Hübener M (2013). Synaptic scaling and homeostatic plasticity in the mouse visual cortex in vivo. *Neuron* **80**, 327–334.
- Larkum ME, Petro LS, Sachdev R & Muckli L (2018). A perspective on cortical layering and layer-spanning neuronal elements. *Front Neuroanat* **12**, 56.
- Liang L & Mendell LM (2013). Bilateral transient changes in thalamic nucleus ventroposterior lateralis after thoracic hemisection in the rat. *J Neurophysiol* **110**, 942–951.
- Lilja J, Endo T, Hofstetter C, Westman E, Young J, Olson L & Spenger C (2006). Blood oxygenation level-dependent visualization of synaptic relay stations of sensory pathways along the neuroaxis in response to graded sensory stimulation of a limb. *J Neurosci* **26**, 6330–6336.
- Manohar A, Foffani G, Ganzer PD, Bethea JR & Moxon KA (2017). Cortex-dependent recovery of unassisted hindlimb locomotion after complete spinal cord injury in adult rats. *Elife* **6**, e23532.
- McLaughlin DF & Juliano SL (2005). Disruption of layer 4 development alters laminar processing in ferret somatosensory cortex. *Cereb Cortex* **15**, 1791–1803.
- Minlebaev M, Colonnese M, Tsintsadze T, Sirota A & Khazipov R (2011). Early  $\gamma$  oscillations synchronize developing thalamus and cortex. *Science* **334**, 226–229.

- Morales-Botello ML, Aguilar J & Foffani G (2012). Imaging the spatio-temporal dynamics of supragranular activity in the rat somatosensory cortex in response to stimulation of the paws. *PLoS One* **7**, e40174.
- Moxon KA, Hale LL, Aguilar J & Foffani G (2008). Responses of infragranular neurons in the rat primary somatosensory cortex to forepaw and hindpaw tactile stimuli. *Neuroscience* **156**, 1083–1092.
- Moxon KA, Oliviero A, Aguilar J & Foffani G (2014). Cortical reorganization after spinal cord injury: always for good?. *Neuroscience* **283**, 78–94.
- Muret D & Makin TR (2020). The homeostatic homunculus: rethinking deprivation-triggered reorganisation. *Curr Opin Neurobiol* **67**, 115–122.
- Nagendran T, Larsen RS, Bigler RL, Frost SB, Philpot BD, Nudo RJ & Taylor AM (2017). Distal axotomy enhances retrograde presynaptic excitability onto injured pyramidal neurons via trans-synaptic signaling. *Nat Commun* **8**, 625.
- Paxinos G & Watson C (2007). *The Rat Brain in Stereotaxic Coordinates* (6th edn). Academic Press, Amsterdam.
- Puig MV, Ushimaru M & Kawaguchi Y (2008). Two distinct activity patterns of fast-spiking interneurons during neocortical UP states. *Proc Natl Acad Sci U S A* **105**, 8428–8433.
- Rigas P & Castro-Alamancos MA (2009). Impact of persistent cortical activity (up states) on intracortical and thalamocortical synaptic inputs. *J Neurophysiol.* **102**, 119–131.
- Rossignol S & Frigon A (2011). Recovery of locomotion after spinal cord injury: some facts and mechanisms. *Annu Rev Neurosci* **34**, 413–440.
- Sakata S & Harris KD (2009). Laminar structure of spontaneous and sensory-evoked population activity in auditory cortex. *Neuron* **64**, 404–418.
- Sanchez-Vives MV & McCormick DA (2000). Cellular and network mechanisms of rhythmic recurrent activity in neocortex. *Nat Neurosci* **3**, 1027–1034.
- Schoffelen JM, Poort J, Oostenveld R & Fries P (2011). Selective movement preparation is subserved by selective increases in corticomuscular gamma-band coherence. *J Neurosci* **31**, 6750–6758.
- Schroeder CE, Mehta AD & Givre SJ (1998). A spatiotemporal profile of visual system activation revealed by current source density analysis in the awake macaque. *Cereb Cortex* **8**, 575–592.
- Schubert D, Kötter R & Staiger JF (2007). Mapping functional connectivity in barrel-related columns reveals layer- and cell type-specific microcircuits. *Brain Struct Funct* **212**, 107–119.
- Siddall PJ & Loeser JD (2001). Pain following spinal cord injury. *Spinal Cord* **39**, 63–73.
- Siddall PJ, McClelland JM, Rutkowski SB & Cousins MJ (2003). A longitudinal study of the prevalence and characteristics of pain in the first 5 years following spinal cord injury. *Pain* **103**, 249–257.
- Soderling TR & Derkach VA (2000). Postsynaptic protein phosphorylation and LTP. *Trends Neurosci* **23**(2), 75–80.
- Sydekum E, Ghosh A, Gullo M, Baltés C, Schwab M & Rudin M (2014). Rapid functional reorganization of the forelimb cortical representation after thoracic spinal cord injury in adult rats. *Neuroimage* **87**, 72–79.
- Tan LL, Oswald MJ, Heintz C, Retana Romero OA, Kaushalya SK, Monyer H & Kuner R (2019). Gamma oscillations in somatosensory cortex recruit prefrontal and descending serotonergic pathways in aversion and nociception. *Nat Commun* **10**, 983.
- Teichert M, Liebmann L, Hübner CA & Bolz J (2017). Homeostatic plasticity and synaptic scaling in the adult mouse auditory cortex. *Sci Rep* **7**, 17423.
- Tutunculer B, Foffani G, Himes BT & Moxon KA (2006). Structure of the excitatory receptive fields of infragranular forelimb neurons in the rat primary somatosensory cortex responding to touch. *Cereb Cortex* **16**, 791–810.
- Veit J, Hakim R, Jadi MP, Sejnowski TJ & Adesnik H (2017). Cortical gamma band synchronization through somatostatin interneurons. *Nat Neurosci* **20**, 951–959.
- Welle CG & Contreras D (2016). Sensory-driven and spontaneous gamma oscillations engage distinct cortical circuitry. *J Neurophysiol* **115**, 1821–1835.
- Wester JC & Contreras D (2012). Columnar interactions determine horizontal propagation of recurrent network activity in neocortex. *J Neurosci* **32**, 5454–5471.
- Wester JC & Contreras D (2013). Differential modulation of spontaneous and evoked thalamocortical network activity by acetylcholine level in vitro. *J Neurosci* **33**, 17951–17966.
- Wilent WB & Contreras D (2004). Synaptic responses to whisker deflections in rat barrel cortex as a function of cortical layer and stimulus intensity. *J Neurosci* **24**, 3985–3998.
- Wrigley PJ, Press SR, Gustin SM, Macefield VG, Gandevia SC, Cousins MJ, Middleton JW, Henderson LA & Siddall PJ (2009). Neuropathic pain and primary somatosensory cortex reorganization following spinal cord injury. *Pain* **141**, 52–59.
- Yague JG, Foffani G & Aguilar J (2011). Cortical hyperexcitability in response to preserved spinothalamic inputs immediately after spinal cord hemisection. *Exp Neurol* **227**, 252–263.
- Yagüe JG, Humanes-Valera D, Aguilar J & Foffani G (2014). Functional reorganization of the forepaw cortical representation immediately after thoracic spinal cord hemisection in rats. *Exp Neurol* **257**, 19–24.
- Yamashita T, Vavladeli A, Pala A, Galan K, Crochet S, Petersen SSA & Petersen CCH (2018). Diverse long-range axonal projections of excitatory layer 2/3 neurons in mouse barrel cortex. *Front Neuroanat* **12**, 33.
- Yuste R & Tank DW (1996). Dendritic integration in mammalian neurons, a century after Cajal. *Neuron* **16**, 701–716.
- Zhang K, Zhang J, Zhou Y, Chen C, Li W, Ma L, Zhang L, Zhao J, Gan W, Zhang L & Tang P (2015). Remodeling the dendritic spines in the hindlimb representation of the sensory cortex after spinal cord hemisection in mice. *PLoS One* **10**, e0132077.

## Additional information

### Data availability statement

The processed dataset obtained from LFP and MUA recordings are freely available on <https://github.com/gnecgroup/S1HLLaminaranalysis.git>. Raw data are available from the corresponding author upon reasonable request.

### Competing interests

The authors declare no competing interests.

### Author contributions

Conceptualization: M.Z., J.M.R. and J.A. Methodology: M.Z., J.M.R., C.M-Q., E.A-C., E.F-L. and J.A. Investigation: M.Z., J.M.R., C.M-Q., E.A-C. and E.F-L. Original draft: J.M.R., M.Z. and J.A. Writing – review and editing: M.Z., C.M-Q., J.M.R., E.A-C., E.F-L., A.O. and J.A. Visualization: M.Z., J.M.R. and J.A. Funding acquisition: J.M.R. A.O. and J.A. All authors have read and approved the final version of this manuscript and agree to be accountable for all aspects of the work in ensuring that questions related to the accuracy or integrity of any part of the work are appropriately investigated and resolved. All persons designated as authors qualify for authorship, and all those who qualify for authorship are listed.

### Funding

This work was supported by Spanish Ministry of Economy and Competitiveness and Ministry of Science, Innovation and

Universities co-funded by FEDER to J.A. (BFU2016-80665-P and PID2019-105020GB), to A.O. (SAF2016-80647-R), to M.Z. (BES2017-082029, predoctoral fellowship FPI-MICINN) and to J.M.R. (RYC2019-026870-I). J.M.R. was also funded by European Union's Horizon 2020 research and innovation programme under the Marie Skłodowska-Curie grant agreement No. 794926.

### Acknowledgements

We thank Dr Casto Rivadulla for helpful comments on the manuscript.

### Keywords

cortical layers, cortical reorganization, forelimb, gamma oscillation, hindlimb, sensory deprivation, sensory-evoked responses, sensory processing, slow-wave oscillation, somatosensory cortex, spinal cord injury

## Supporting information

Additional supporting information can be found online in the Supporting Information section at the end of the HTML view of the article. Supporting information files available:

### Peer Review History Statistical Summary Document